Modeling carbon and silicon cycling in the equatorial Pacific

Masahiko Fujii[1,2,*] and Fei Chai[1]

[1]School of Marine Sciences, 5706 Aubert Hall, University of Maine, Orono, ME 04469-5706, USA

[2]Now at Sustainability Governance Project, Hokkaido University, Sapporo, Hokkaido 060-0809, Japan

[*]Corresponding author. Tel: +81-11-706-4536; Fax: +81-11-706-4534

E-mail: mfujii@sgp.hokudai.ac.jp (M. Fujii)

Abstract

The equatorial Pacific is a region of significant particulate inorganic carbon (PIC) and biogenic silica sedimentation, the majority of which is carried out by coccolithophorids and diatoms. We developed an ecosystem model that explicitly includes three phytoplankton functional groups (picoplankton, coccolithophorids, and diatoms), two zooplankton functional groups (microzooplankton and mesozooplankton), nutrients (nitrate NO_3, ammonium NH_4, and silicate $Si(OH)_4$), detritus (particulate organic matter, biogenic silica, and PIC), total alkalinity, total CO_2, and partial pressure of CO_2 at the surface water (pCO_{2sea}). The model is capable of reproducing many biogeochemical features for the region, such as high-nutrient low-chlorophyll condition, significant exposure of phytoplankton under grazing controls by zooplankton, and large CO_2 release to the atmosphere. The export ratio of PIC to particulate organic carbon (rain ratio) to the deep water was 0.16, higher than the global-mean values, implying predominant PIC sedimentation in the equatorial Pacific upwelling region. Comparison between calcification and no-calcification model results indicates that when coccolithophorids were present, the community interatctions actually induced more diatom biomass, export fluxes of detritus, and CO_2 release to the atmosphere. The model results show remarkable calcification in the subsurface layers, which suggests more field data on calcification processes are needed. Increase of source (120m depth) $Si(OH)_4$ concentration associated with the tropical instability waves lead to a linear increase in biogenic silica export. Higher $Si(OH)_4$ concentration stimulated diatom growth, which caused a decrease in picoplankton because feeding pressure by mesozooplankton switched from picoplankton's grazer, microzooplankton, to the abundant diatoms. Surface coccolithophorid biomass had its maximum at intermediate source $Si(OH)_4$ concentrations as a result of higher grazing pressure on coccolithophorids and higher NO_3 regulation on coccolithophorid growth, with lower and higher source $Si(OH)_4$ concentrations, respectively. Surface total alkalinity had its minimum and TCO_2 had its

maximum at intermediate source $Si(OH)_4$ concentrations. The two effects on pCO_{2sea} resulted in maximum CO_2 release to the atmosphere and PIC export to the deep water, with nearby standard source $Si(OH)_4$ concentration of 7.5 [mmolSi m^{-3}]. The enhanced changes in biogenic silica export flux than in surface diatom biomass, confirmed by the model sensitivity study, suggests sedimented detritus under the equatorial Pacific upwelling region acts as an amplifier of changes in surface properties. The model results suggest that physical forcings, such as tropical instability waves, Kelvin waves, and La Niña, which are capable of changing $Si(OH)_4$ and iron concentrations in the euphotic zone, significantly affect both carbon and silicon fluxes in the region.

1. Introduction

1.1 Calcification in the equatorial Pacific

Calcifying plankton have a great role in oceanic carbon cycling and global climate change because of particulate inorganic carbon (PIC) shell production resulting in reduced alkalinity and CO_2 release to the atmosphere, the ballasting effect of carbonate minerals, and the packaging effect of promoting the transfer of organic carbon to the deep sea (*e.g.* Armstrong *et al.*, 2002; Francois *et al.*, 2002).

Previous studies have indicated that the majority (80%) of global marine biogenic carbonate precipitation is carried out by coccolithophorids (Deuser and Ross, 1989; Fabry, 1989; Westbroek *et al.*, 1989) through their production of PIC coccoliths. Coccolithophorids acts as a significant biotic source of dimethyl sulfide (DMS) for the atmosphere and may influence regional albedo via increased cloud formation (*e.g.* Bates *et al.*, 1987; Charlson *et al.*, 1987; Brown and Yoder, 1994). The coccolithophorid bloom affects physical environments through changing albedo due to their unique light scattering properties, and biogeochemical processes from lower to higher trophic levels. The progressive increase in atmospheric CO_2 concentrations predicted for the next few decades will decrease the production of PIC in the surface ocean (Riebesell *et al.*, 2000; Orr *et al.*, 2005), and thus this response could potentially act as a negative feedback on atmospheric CO_2 levels (Iglesias-Rodríguez *et al.*, 2002).

Although satellite-based estimates of coccolithophore blooms appear in high-latitude oceans, and the relative paucity of such blooms in the tropics (*e.g.*, Holligan *et al.*, 1983; Brown and Yoder, 1994; Brown, 1999; Iglesias-Rodríguez *et al.*, 2002), the equatorial Pacific is known as a region of significant PIC sedimentation (van Andel, 1975), which represents 12-19% of global PIC production, and is on the same order of magnitude as new production in this region (Chavez and Barber, 1987; Balch and Kilpatrick, 1996). The equatorial Pacific is a largest natural CO_2 source to the atmosphere,

and therefore, change in calcification in the region can significantly impact on the global carbon cycling.

Calcification in the equatorial Pacific is poorly understood from ecological and biogeochemical perspectives because direct field estimates of calcification are few (Balch and Kilpatrick, 1996). Ecosystem modeling can help us to fill the gaps in observations and interpret observed results. Several ecosystem models have incorporated calcifying plankton as well as carbonate system (*e.g.* Fujii *et al*., 2002; Moore *et al*., 2002; Pätsch *et al.*, 2002; Yamanaka *et al*., 2004). However, they all assumed a constant composition ratio of coccolithophorids to total phytoplankton or a constant ratio of calcification to net community production. Only very few previous studies have incorporated calcifying plankton in their models as an independent state variable (Pasquer *et al*., 2005; Buitenhuis *et al*., 2006).

1.2 Silicification in the equatorial Pacific

The equatorial Pacific upwelling region is known as one of the major high-nutrient, low-chlorophyll (HNLC) regions. This oceanic region is also characterized by permanently lower $Si(OH)_4$ than NO_3 concentration. For example, typical source (120m depth) concentration is 7.5 [mmolSi m^{-3}] for $Si(OH)_4$ and 12.5 [mmolSi m^{-3}] for NO_3, which leads to lower surface $Si(OH)_4$ than NO_3 concentration and potential $Si(OH)_4$ limitation on the diatom growth (*e.g.*, Ku *et al.*, 1995; Dugdale *et al.*, 1995; Dugdale and Wilkerson, 1998). However, field data in this region have shown that the source $Si(OH)_4$ concentration ranges substantially from 3 to 13 [mmolSi m^{-3}] (*e.g.*, Dugdale *et al.*, 2002). This means that the $Si(OH)_4$ limitation on the diatom growth and, therefore, phytoplankton community composition, could change widely in response to the source $Si(OH)_4$ concentration. Recent iron enrichment experiments in the equatorial Pacific have shown that iron as well as $Si(OH)_4$

concentration are crucial factors determining diatom growth and its biomass accumulation (*e.g.*, Martin *et al.*, 1994; Coale *et al.*, 1996; Price *et al.*, 1994; Sanderson *et al.*, 1995).

Both $Si(OH)_4$ and iron in the surface water are primarily supplied by upwelling from the deep water (*e.g.*, Chavez *et al.*, 1991; Dugdale *et al.*, 2002), although less is known of the distribution of iron, its form, and cycling. The nutrient concentrations change with physical forcing that varies on different time scales from days to years. Several previous studies have investigated biogeochemical responses in the equatorial Pacific to the non steady-state event associated with the passage of the tropical instability waves (TIWs), La Niña and Kelvin waves (*e.g.*, Barber *et al.*, 1996; Foley *et al.*, 1996; Dunne *et al.*, 1999; Dugdale *et al.*, 2002). The passage of the TIWs lifts isopycnals, presumably elevating $Si(OH)_4$ and iron concentrations, as well as diatom production in the euphotic zone for a short period (*e.g.*, Flament *et al.*, 1996: Archer *et al.*, 1997). The passage of Kelvin waves, by contrast, depresses the thermocline (*e.g.*, Kessler and McPhaden, 1995), decreasing inputs of iron to the euphotic zone.

Although the concept of non steady-state is important in understanding equatorial biogeochemical cycles (*e.g.*, Dunne *et al.*, 1999), the total impact of the TIWs and Kelvin waves and their frequency still remains uncertain mainly due to a paucity of field data. In parallel, several modeling studies have examined the biological responses to enhanced nutrients by the TIWs. Using a ten-compartment ecosystem model that fully incorporates silicon cycling, and representing iron enrichment by changing two photosynthetic parameters of the diatoms, Chai *et al.* (2002) reproduced several ecological behaviors similar to those observed during the second mesoscale iron enrichment experiment (IronExII; at 3.5ºS, 104ºW). These behaviors included a rapid increase in diatom growth and biomass, termination of the iron-induced diatom bloom due to exhaustion of available iron and $Si(OH)_4$, and increased mesozooplankton population as a grazer on diatoms. Using the same ecosystem model, Dugdale *et al.* (2002) suggested that the stability of the equatorial system with its narrow range

of biological and chemical variables is conferred by the action of diatoms providing food for mesozooplankton, whose grazing also depletes picoplankton. They also suggested that diatoms increase while picoplankton population and NO_3 consumption decrease with source $Si(OH)_4$ increases. As a result, a maximum surface total carbon dioxide (TCO_2) and increased CO_2 flux to the atmosphere appear at intermediate source $Si(OH)_4$ concentrations.

1.3. Objective of this study

To elucidate factors that affect calcification and PIC sedimentation in the equatorial Pacific, we propose to address the roles of coccolithophorids and other phytoplankton and zooplankton groups that affect coccolithophorids. We develop and use an ecosystem model incorporating coccolithophorids, PIC, and total alkalinity. The model performance is tested by applying the model to the equatorial Pacific upwelling region. Model sensitivity analysis to biogeochemical parameters (Experiment 1) is conducted to understand dominant biological processes in the newly-developed ecosystem model.

To examine responses of the biogeochemistry in the equatorial Pacific to changes in $Si(OH)_4$ and iron concentrations in the euphotic zone induced by the TIWs, we conduct a model sensitivity study (Experiment 2). In Experiment 2, we investigate model sensitivity to the source (120m depth) $Si(OH)_4$ concentrations under the steady-state conditions. We compare all the model results to those with no-calcification model simulation, as well as the JGOFS EqPac field data.

2. Experimental design

2.1. Model description

We added three prognostic variables, namely calcifying phytoplankton (coccolithophorids, or P3), total alkalinity (TAlk), and particulate inorganic carbon (PIC) (Fig. 1), as well as the other phytoplankton functional groups (picoplankton (P1) and diatoms (P2)), zooplankton (microzooplankton (Z1) and mesozooplankton (Z2)), nutrients (NO_3, NH_4 and $Si(OH)_4$), detritus (particulate organic nitrogen and carbon (PON and POC) and biogenic silica ($bSiO_2$)), total CO_2 (TCO_2), and partial pressure of CO_2 in the surface water (pCO_{2sea}) which were embedded in a 1-D marine ecosystem model (Chai *et al.*, 2002). The phytoplankton and zooplankton were separated by their functional groups, not only by their size but also according to their growth and vulnerability to grazing. All the phytoplankton take up NO_3, NH_4, and TCO_2 by the photosynthesis. The diatoms also utilize $Si(OH)_4$ for their silicification process and the coccolithophorids take up TAlk as well as TCO_2 for its calcification process. The microzooplankton graze on picoplankton. The mesozooplankton feed on diatoms, coccolithophorids, microzooplankton and PON. The explicit representation of Talk and TCO_2 in the model allows us to calculate pCO_{2sea} and the air-sea CO_2 flux. The phytoplankton carbon-chlorophyll-a ratio by weight was fixed to 50. The governing equations and formulations of biogeochemical processes were denoted in Appendix.

The model was applied to 5°S-5°N, 90-180°W (the "Wyrtki Box", Wyrtki, 1981; Chai *et al.*, 2002). The physical forcing is the same, and most of the biogeochemical parameter values are the same as Chai *et al.* (2002) (Table 1). The parameter values were obtained to reproduce the temporally-averaged observed constituents such as nutrient concentrations and new production in the euphotic layer (Chai *et al.*, 1996), which varied between El Niño and non-El Niño periods (*e.g.* McCarthy *et al.*, 1996). Steady-state results obtained by running the model up to 1000 days with the

constant vertical velocity and diffusivity were used.

2.2. Data description

Datasets were used to tune the biological parameters and to compare with model outputs. Datasets used in this study are as follows: the U.S. JGOFS EqPac observations in February-March (Survey I; TT007), March-April (Time series I; TT008), August-September (Survey II; TT011) and October (Time series II; TT012) of 1992 (*e.g.* Murray *et al*., 1995, 1996 and 1997; Balch and Kilpatrick, 1996; Barber *et al.*, 1996); the France JGOFS fluxes in the Pacific transect (FLUPAC) in October of 1994 (Le Borgne *et al*., 1995 ; Rodier and Le Borgne, 1997); the Oligotrophie en Pacifique (OLIPAC) in November 1994 (Rainbault *et al*.,1999); the U.S. Zonal Flux transect (Zonal Flux) in April-May of 1996 (Dunne *et al.*, 1999); the Etude du Broutage en Zone Equatoriale (EBENE) cruise in October-November of 1996 (Le Borgne *et al.*, 1998; Leynaert *et al.*, 2001); the World Ocean Database 2001 (WOD01; Conkright *et al*., 2002); the IronExII field data (Coale *et al.*, 1996; Landry *et al.*, 2000).

2.3. Comparison between calcification and no-calcification model simulations

To elucidate effects of newly-introduced coccolithophorids and its calcification processes on the entire biogeochemistry in the equatorial Pacific upwelling region, we compared model results with and without components and processes that were relevant to the calcification. In the no-calcification model simulation, we have excluded state variables of coccolithophorids and PIC. The no-calcification model structure was identical to that in Chai *et al.* (2002) and Dugdale *et al.* (2002). Small differences in the model results from the previous studies were attributed to different values in several biogeochemical parameters between the studies (Table 1; Chai *et al.* 2002).

3. Results

3.1. Calcification model

The modeling results reasonably reproduced the measured vertical features in the biogeochemistry in the equatorial Pacific, such as consistently higher NO_3 than $Si(OH)_4$ concentration (solid line in Fig. 2 (d), (f)). The modeled picoplankton (P1) was more abundant than diatoms (P2) and coccolithophorids (P3) (solid lines in Fig. 2 (a)), which has been suggested from the observations (Bidigare and Ondrusek, 1996). The modeled vertically-averaged phytoplankton abundance was 0.15 [mmolN m^{-3}] for picoplankton, 0.06 [mmolN m^{-3}] for diatoms, and 0.03 [mmolN m^{-3}] for coccolithophorids (Table 2). The percentage of diatoms in the total modeled phytoplankton biomass was 24%, which was slightly higher but was consistent with the observed range of 5-20% (Bidigare and Ondrusek, 1996).

The modeled vertically-averaged biomass was 0.13 [mmolN m^{-3}] for microzooplankton (Z1) and 0.28 [mmolN m^{-3}] for mesozooplankton (Z2) (Table 2), indicating that mesozooplankton was more plentiful than the other plankton, and therefore, possibly high grazing or predation pressure by mesozooplankton in the equatorial Pacific upwelling region. The abundance in the modeled zooplankton rapidly decreased with depth (solid lines in Fig. 2 (c)), as a result of their grazing and predation being dependent on biomass of their prey (Appendix A.2).

The modeled NO_3 and $Si(OH)_4$ increased with depth (solid line in Fig. 2 (d), (f)), resulting from nutrient uptake by phytoplankton near the surface and remineralization of PON and $bSiO_2$ below the depth. At 120m, $Si(OH)_4$ concentration was 7.5 [mmolSi m^{-3}], whereas NO_3 concentration was 12.0 [mmolN m^{-3}], and these values are close to the observed climatological data, respectively (*e.g.* Levitus *et al*., 1993; Murray *et al*., 1995; Chai *et al*., 2002; Dugdale *et al*., 2002). The surface concentration was 6.1 [mmolN m^{-3}] in NO_3 and 3.1 [mmolSi m^{-3}] in $Si(OH)_4$. The model captured the observed

subsurface maximum of NH_4 concentration (solid line in Fig. 2 (e); Murray *et al.*, 1995). The subsurface NH_4 maximum is due to higher uptake rate of NH_4 near the surface mainly by picoplankton which has relatively smaller half-saturation constant for NH_4 uptake (0.1 [mmolN m^{-3}]) than the other phytoplankton has (1.0 [mmolN m^{-3}]) (Table 1).

The modeled TCO_2 had similar vertical profile as of nutrients, increasing with depth (solid line in Fig. 2 (h)), as a result of TCO_2 uptake by phytoplankton growth and calcification by coccolithophorids in the upper layer and decomposition of POC and PIC in the lower layer. The TAlk was only changed by the calcification process, *i.e.* shell formation by coccolithophorids in the upper layer and dissolution of PIC in the lower layer, so the vertical change was smaller in TAlk than in TCO_2 (solid lines in Fig. 2 (g), (h)). The pCO_{2sea} depends on TAlk as well as the temperature, salinity and TCO_2 in the surface water, so it could be estimated more precisely than with previous models which did not explicitly incorporate change of TAlk (*e.g.* Chai *et al.*, 2002). The pCO_{2sea} was 401 [µatm] (Table 3), close to the observed values (*e.g.* Feely *et al.*, 1997). The pCO_{2sea} was much higher than the partial pressure of CO_2 in the atmosphere of 357 [µatm] (Appendix A.1; Chai *et al.*, 2002), suggesting the equatorial Pacific upwelling region as a large CO_2 source to the atmosphere, as the observed.

The modeled net community production was obtained by multiplying the nitrogen changes in the water column by the Redfield stoichiometric ratio of 6.625 (Table 1). The modeled vertical profile of net community production reproduced well the observations (Fig. 3 (a)), implying that fixing a phytoplankton carbon:nitrogen ratio is a good assumption in this region. The modeled calcification in the euphotic zone (Fig. 3 (b)) was lower than the field data during EqPac Survey II (TT011; in August 1992) in which the measured calcification was considered to be higher than the normal conditions (Balch and Kilpatrick, 1996). The modeled column-integrated ratio of calcification to net community production was 0.06, lies on a lower end of the observed range from 0.03 to 0.12 during EqPac Survey

II (Balch and Kilpatrick, 1996). A higher ratio of the calcification to the net community production could be reproduced by changing a few model parameter values which are relevant to coccolithophorids, such as the maximum specific growth rate of coccolithophorids ($\mu 3_{max}$) and the half-saturation constant for NH_4 uptake by coccolithophorids (K_{P3_NH4}), as described in the next subsection.

The modeled $bSiO_2$ production with depth showed a pattern similar to that of the net community production although the modeled $bSiO_2$ production decreased more rapidly with depth (Fig. 3 (a), (c)). The modeled vertical profile reproduced the field data (Leynaert *et al.*, 2001), but the model overestimated the field results in the lower layer. Unlike the calcification data, the $bSiO_2$ data were collected during the EBENE cruise in October-November 1996, which took place during a "neutral scenario" between El Niño and La Niña (Leynaert *et al.*, 2001). Therefore, the $bSiO_2$ data can be considered to be normal, and the model-data misfit was probably caused by other biological factors such as a vertical change in the diatom Si:N uptake ratio that was not considered in the present model.

The modeled $bSiO_2$:POC production ratio remarkably decreased with depth, from 0.03 at the surface to nearly zero at 120m depth, following the rapid decrease in diatom biomass with depth (solid line in Fig. 2 (a)) as observed (*e.g.* Barber *et al.*, 1996). The modeled PIC:POC production ratio, by contrast, was relatively similar with depth but had its maximum of 0.07 around 50m depth (Fig. 3 (d)). The increased dominancy of coccolithophorids in the subsurface layers resulted from its strategy to seek for NH_4 which was rapidly consumed by picoplankton in the surface water (solid line in Fig. 2 (e)). This implies that the calcification in the subsurface layers, which cannot be detected by satellite observations, plays a considerable role in significant PIC sedimentation in the equatorial Pacific.

The modeled export flux of PON, POC, $bSiO_2$, and PIC at 120m depth was 0.58 [mmolN m^{-2} day^{-1}], 3.84 [mmolC m^{-2} day^{-1}], 1.46 [mmolSi m^{-2} day^{-1}], and 0.60 [mmolC m^{-2} day^{-1}], respectively

(Table 4). All the export fluxes of PON, POC and $bSiO_2$ lie within the observed wide ranges of 0.38-4.65 [mmolN m^{-2} day^{-1}], 0.6-20 [mmolC m^{-2} day^{-1}] and 0.05-3.9 [mmolSi m^{-2} day^{-1}], respectively. The PIC:POC export ratio (rain ratio) in the equatorial Pacific upwelling region was 0.16 in this study (Table 4). This is relatively higher than recent estimates of 0.05-0.08 for the global-mean rain ratio (*e.g.* Yamanaka and Tajika, 1996; Najjar and Orr, 1998; Milliman *et al.*, 1999; Sarmiento *et al.*, 2002; Fujii *et al.*, 2005a), implying notable PIC export in the equatorial Pacific compared to the global ocean, as reported by Balch and Kilpatrick (1996).

The modeled $bSiO_2$:PON export ratio was 2.52 (Table 4), which lies between the maximum ratio of nearly 4 obtained by Dugdale *et al*. (2002) and other sediment trap data of 0.10-1.25 (Dunne *et al.*, 1999). Recent data show that bacterial protease activity accelerates the dissolution of $bSiO_2$ in the euphotic zone (Bidle and Azam, 1999), and that such process is strongly dependent on water temperature (Bidle *et al.*, 2002, 2003). Other previous studies suggested that the dissolution of $bSiO_2$ is correlated to the percentage of dead diatoms, and that other factors controlling $bSiO_2$ dissolution rate besides water temperature, such as differences in organic coatings that protect against $bSiO_2$ dissolution between live and dead diatoms, are probably required (Beucher *et al.*, 2004; Fujii and Chai, 2005). These factors, which were not taken into account in the present model, probably contributed to the large spatial and temporal variation among the observed $bSiO_2$:PON export ratios and to regard sedimented biogenic silica under the equatorial upwelling area as an amplifier of changes in surface properties (Dugdale *et al.*, 2002).

3.2. Comparison with no-calcification model results

We compared the standard model experimental results with and without coccolithophorids and its calcification processes (hereafter calcification and no-calcification model simulation, respectively).

The no-calcification model results were obtained by eliminating all the parameters that are associated with coccolithophorids and its calcification processes and by modifying the grazing preference by mesozooplankton properly (Table 1).

The model results showed that surface diatom biomass was less than half in the no-calcification model simulation, although the diatom specific growth rate (diatom growth rate divided by its biomass) was 23% higher due to higher $Si(OH)_4$ concentration (Table 3; Fig. 2 (a), (f)). This results from absence of grazing pathway by mesozooplankton on coccolithophorids and subsequently higher grazing pressure on diatoms by mesozooplankton (by a factor of 1.3 in terms of the specific grazing rate, grazing rate divided by prey's biomass) in the no-calcification model simulation (Table 3). The absence of coccolithophorids in the no-calcification model simulation yielded enhancement of the other feeding pathways by mesozooplankton, namely predation on microzooplankton and grazing on PON as well, by a factor of 1.6 and 1.8, respectively (Table 3). As a result, mesozooplankton biomass was 26% higher in the no-calcification model simulation (Table 3; Fig. 2 (c)). The substantially enhanced predation on microzooplankton by mesozooplankton in the no-calcification model simulation slightly lowered grazing pressure on picoplankton by microzooplankton, which lead to 33% higher picoplankton biomass regardless of its lower specific growth rate due to lower NH_4 and NO_3 concentrations than in the calcification model simulation (Table 3; Fig. 2 (a), (d), (e)).

Compared to the change in each phytoplankton biomass between the calcification and no-calcification model simulations, the total phytoplankton biomass in the surface water was similar between the two models, because the absence of coccolithophorids and the lower diatom biomass in the no-calcification model simulation were partly compensated by the higher picoplankton biomass (Table 3; Fig. 2 (a), (b)). The export flux of PON or POC, which is generated from phytoplankton mortality

and fecal pullet, was similar as well (changing only by 12%; Table 4). On the other hand, the $bSiO_2$ export was lower in the no-calcification model simulation by 49% (Table 4). Same as the relationship between the surface NO_3 and $Si(OH)_4$, the change was relatively smaller in surface TCO_2 than in TAlk between the two models (Table 3; Fig. 2 (g), (h)). The higher TAlk and lower TCO_2 causes lower pCO_{2sea} in the no-calcification model simulation by 47μatm (Table 3), which was primarily affected by the increase in TAlk.

4. Discussion

4.1. Sensitivity to biogeochemical parameters (Experiment 1)

We tested model sensitivity to each biogeochemical parameter by changing the parameter value from 0.5 to 1.5 times the standard value (Table 1). We found the model results, *i.e.*, surface plankton abundance, concentrations of nutrients, TAlk and TCO_2, pCO_{2sea}, and export fluxes of PON, $bSiO_2$ and PIC, were especially sensitive to changes in six model parameters relevant to grazing or predation by zooplankton, namely the maximum grazing and/or predation rates by zooplankton ($G1_{max}$ and $G2_{max}$), the half-saturation constants for zooplankton ingestion ($K1_{gr}$ and $K2_{gr}$), the mesozooplankton excretion rate to NH_4 (reg_2), and the mesozooplankton specific mortality rate (γ_2) (Table 5). This suggests that the phytoplankton in the equatorial Pacific upwelling area is universally and severely exposed under the top-down (grazing) control by zooplankton. This is consistent with the observed results that grazing has been invoked as the control on loss rates (*e.g.* Walsh, 1976; Landry *et al.*, 1997; Dugdale *et al.*, 2002).

The maximum grazing or predation rate by mesozooplankton ($G2_{max}$) was the most significant parameter to determine surface diatoms, coccolithophorids, $Si(OH)_4$, TAlk, TCO_2, and export fluxes of PON and PIC (Table 5; Fig. 4). The lower $G2_{max}$ caused lower grazing pressure on diatoms and coccolithophorids and subsequently higher diatom and coccolithophorid biomass, which lead to higher export fluxes of POC, $bSiO_2$ and PIC, and lower TAlk and TCO_2 (Fig. 4 (a), (b), (c), (d), (f)). The simultaneous decrease in TAlk and TCO_2 (238 [mmol m^{-3}] and 149 [mmolC m^{-3}], respectively) with $G2_{max}$ decrease compensated each other in terms of pCO_{2sea} change, which yielded pCO_{2sea} decrease of 137 [μatm] (Fig. 4 (e)), significant but relatively small compared to the individual changes in TAlk and TCO_2.

The maximum grazing rate on picoplankton by microzooplankton ($G1_{max}$) was the most

effective parameter in determining surface picoplankton biomass and NO_3 (Table 5). Two phytoplankton-related parameters (the initial slope of P-I curve (α) and the maximum specific growth rate of picoplankton (μ_{1max})) also controlled the model results, but less broadly than the zooplankton-related parameters above did (Table 5). The surface TAlk and TCO_2 varied by 21-45 [mmol m^{-3}] and 53-81 [mmolC m^{-3}], respectively, by changing one of the three parameter values (Table 5; Fig. 5 (a), (b)). These changes were relatively small compared those brought by $G2_{max}$ change of 238 [mmol m^{-3}] and 149 [mmolC m^{-3}], respectively. However, surface TAlk and TCO_2 changed in a different way with parameter values, *i.e.*, surface TAlk increased and TCO_2 decreased with parameter values of α and μ_{1max}, and vice versa for $G1_{max}$. This is the reason why the pCO_{2sea} change by changing these parameter values was relatively large (184, 147 and 160 [μatm] for α, μ_{1max} and $G1_{max}$, respectively; Table 5; Fig. 5 (c)).

The surface coccolithophorid biomass and the export PIC flux at 120m depth were sensitive to many parameters (Table 5). For example, a few parameters like the maximum specific growth rates of coccolithophorids ($\mu 3_{max}$) and the half-saturation constant for NH_4 uptake by coccolithophorids (K_{P3_NH4}) specialized to control the two model state variables. This means that the modeled coccolithophorids and PIC could change in a sensitive and complicated way with a narrow range of the parameter values. For more realistic simulation of carbon cycling in this region, we need further field data, especially for vertical profiles of POC, PIC, coccolithophorid biomass and its composition ratio for the phytoplankton community.

The model sensitivity study to the five parameters of α, $\mu 1_{max}$, $\mu 3_{max}$, $G1_{max}$ and $G2_{max}$ revealed that the $bSiO_2$:PON export ratio and the PIC:POC export ratio (rain ratio) at 120m depth could vary by 0.40-2.83 and 0.00-0.56, respectively (Fig. 6). Considering that the observation-based estimates of the global rain ratio vary from 0.05 to 0.25 (*e.g.* Fujii *et al.*, 2005a) and excluding the model results in

which the rain ratio was out of the range (Fig. 6 (b)), we obtained a range of 1.51-2.75 for the $bSiO_2$:PON export ratio (Fig. 6 (a)).

4.2. Sensitivity to source $Si(OH)_4$ concentration (Experiment 2)

Experiment 2 is similar to the experiment conducted by Dugdale *et al.* (2002), *i.e.*, the source (120m depth) $Si(OH)_4$ concentration was varied from 3.0-15.0 [mmolSi m^{-3}], corresponding to the full range of JGOFS equatorial values of 3-13 [mmolSi m^{-3}] (Dugdale *et al.*, 2002). The NO_3 concentration at 120m depth was held constant at 12.0 [mmolN m^{-3}].

4.2.1. Calcification model simulation

With source (120m depth) $Si(OH)_4$ concentration increases, surface $Si(OH)_4$ concentration increased linearly from 1.8 to 6.6 [mmolSi m^{-3}] (solid line in Fig. 7 (f)). The surface $Si(OH)_4$ increase enhanced surface diatom growth (Fig. 8 (b)) and increased surface diatom biomass by a factor of 4.3 (solid green line in Fig. 7 (a)). The surface diatom increase resulted in a remarkable switch in feeding by mesozooplankton from microzooplankton to diatoms as the source $Si(OH)_4$ increased (Fig. 8 (b), (d)). The declined predation on microzooplankton by mesozooplankon enhanced grazing pressure on picoplankton by microzooplankton (Fig. 8 (a)), causing a decrease in surface picoplankton biomass with source $Si(OH)_4$ increase (solid line in Fig. 7 (a)). The decrease in surface picoplankton biomass was more rapid with lower source $Si(OH)_4$ concentrations.

The surface diatom increase with source $Si(OH)_4$ concentration also yielded a slight switch in grazing by mesozooplankton from coccolithophorids to diatoms (Fig. 8 (b), (c)), which increased surface coccolithophorid biomass (Fig. 7 (b)). The surface coccolithophorid biomass had its maximum at source $Si(OH)_4$=8-9 [mmolSi m^{-3}] and then decreased with higher source $Si(OH)_4$ concentrations due

to slight NO_3 regulation on the coccolithophorid growth as the result of higher diatom growth (solid lines in Fig. 7 (b), (e), and Fig. 8 (b), (c)). The total phytoplankton biomass in the surface water had its minimum at source $Si(OH)_4$=5 [mmolSi m^{-3}] (solid line in Fig. 7 (c)). The phytoplankton composition ratio in the surface water was 80, 11, and 9% at source $Si(OH)_4$=3 [mmolSi m^{-3}]; 52, 33, and 15% at source $Si(OH)_4$=7.5 [mmolSi m^{-3}]; and 46, 42, and 12% at source $Si(OH)_4$=15 [mmolSi m^{-3}] (solid lines in Fig. 7 (d)), indicating substantial increase in diatoms and decrease in picoplankton and relatively similar coccolithophorid biomass with source $Si(OH)_4$ increase.

Surface TAlk is taken up by the coccolithophorids' calcification process. Hence, TAlk had its minimum with source $Si(OH)_4$=7-8 [mmolSi m^{-3}] at which surface coccolithophorids biomass had its maximum (solid lines in Fig. 7 (b), (g)). The surface TCO_2, which is taken up by both phytoplankton growth and calcification, had its maximum with source $Si(OH)_4$=7 [mmolSi m^{-3}], mainly as the result of the lowest total phytoplankton biomass in the surface water (solid line in Fig. 7 (c) and (h)). The pCO_{2sea} decreases with TAlk increase and increases with TCO_2 increase. The two opposite changes in the pCO_{2sea} by TAlk and TCO_2 varies formed a maximum pCO_{2sea} with source $Si(OH)_4$=7 [mmolSi m^{-3}] (solid line in Fig. 7 (i)). The pCO_{2sea} changed from 357 to 401 [μatm], in a similar range as observed (*e.g.*, Feely *et al.*, 1997).

With source $Si(OH)_4$ increase, or with surface diatom biomass increase, the modeled $bSiO_2$ export at 120m depth dramatically increased by a factor of 6.6 from 0.38 to 2.52 [mmolSi m^{-2} day^{-1}] (solid line in Fig. 9 (a)). The modeled PON or POC export at 120m depth also increased with source $Si(OH)_4$ concentrations, but only slightly by a factor of 1.2. The modeled PIC export at 120m depth changed by a factor of 1.6 from 0.38 to 0.60 [mmolC m^{-2} day^{-1}] and had its maximum around the standard source $Si(OH)_4$ concentration of 7.5 [mmolSi m^{-3}] (Fig. 9 (b)). The difference in the curve among PON or POC, $bSiO_2$, and PIC appeared because PON or POC was produced by fecal pellet and

phytoplankton mortality, while $bSiO_2$ and PIC were only produced by diatoms and coccolithophorids, respectively. The modeled $bSiO_2$:PON export ratio at 120m depth changed by a factor of 5.6, from 0.7 to 3.9 with source $Si(OH)_4$ concentrations (solid line in Fig. 9 (c)). The larger extent of change in $bSiO_2$ export with source $Si(OH)_4$ concentrations (solid line in Fig. 9 (a)) than of surface diatom biomass (by a factor of 4.3; solid line in Figs. 7 (a)) suggests sedimented detritus under the equatorial Pacific upwelling region act as an amplifier of changes in surface properties (Dugdale *et al.*, 2002). The modeled PIC:POC export ratio (rain ratio) at 120m depth changed by a factor of 1.5 from 0.11 to 0.16, and its maximum appeared at source $Si(OH)_4$=7, close to the standard concentration of 7.5 [mmolSi m^{-3}] (Fig. 9 (d)).

The model results showed that pCO_{2sea} and export PIC:POC and $bSiO_2$:PON ratios, all of which are excellent indices for assessing abilities of CO_2 release to the atmosphere and detritus sedimentations in the equatorial Pacific, were sensitive to source $Si(OH)_4$ concentrations. In particular, the carbonate system in the surface water, PIC export, and the rain ratio at 120m depth had their peaks near the standard source $Si(OH)_4$ concentration of 7.5 [mmolSi m^{-3}], suggesting sensitive change in the CO_2 release to the atmosphere within a narrow range of the source $Si(OH)_4$ concentrations presumably caused by the physical forcing in the equatorial Pacific upwelling region.

4.2.2. Comparison with no-calcification model results

By eliminating coccolithophorids in the no-calcification model simulation, grazing on diatoms by mesozooplankton was elevated in order to compensate the missing grazing pathway from coccolithophorids to mesozooplankton (Fig. 10 (b)). Therefore, the diatom biomass was lower and the $Si(OH)_4$ concentration was higher in the no-calcification model simulation (Fig. 7 (a), (f)). For the same reason, the predation on microzooplankton by mesozooplankton was also elevated in the

no-calcification model simulation (Fig. 10 (c)). The greater predation on microzooplankton by mesozooplankton alleviated grazing pressure on picoplankton by microzooplankton (Fig. 10 (a)), which yielded higher surface picoplankton biomass with lower source $Si(OH)_4$ concentrations in the no-calcification model simulation (Fig. 7 (a)). As the source $Si(OH)_4$ concentration increased, the surface diatom biomass increased, which lead to dominant mesozooplankton's grazing on diatoms over predation on microzooplankton, in both models (Figs. 7 (a) and 10 (b), (c)). But the amplitude of decrease in predation on microzooplankton with source $Si(OH)_4$ concentrations was greater in the no-calcification model simulation (Fig. 10 (c)), which yielded greater amplitude of increase in grazing on picoplankton by microzooplankton and decrease in the surface picoplankton biomass (Figs. 7 (a) and 10 (a)) than in the calcification model simulation. The surface diatom biomass was constantly lower in the no-calcification model simulation because of substantially higher grazing pressure by mesozooplankton than seen in the calcification model simulation (Figs. 7 (a) and 10 (b)).

The total phytoplankton biomass in the surface water decreased with source $Si(OH)_4$ increase in the no-calcification model simulation (dotted line in Fig. 7 (c)), which was followed by increases in surface NO_3 and TCO_2 concentrations (dotted line in Fig. 7 (e), (h)). The surface TAlk was higher and was kept constant in the no-calcification model simulation (dotted line in Fig. 7 (g)). Therefore, the pCO_{2sea} change in the no-calcification model simulation, increasing linearly with source $Si(OH)_4$, from 326 to 380 [μatm], was primarily controlled by the surface TCO_2 change (dotted line in Fig. 7 (h), (i)). The lower surface total phytoplankton and diatom biomass in the no-calcification model simulation resulted in lower export fluxes of PON or POC and $bSiO_2$, and a lower $bSiO_2$:PON export ratio than in the calcification model simulation (Figs. 7 (a), (c) and 9 (a), (c)).

4.3. Comparison with field data

The passage of the TIWs during the JGOFS TT012 cruise gave a natural experiment of how the surface nutrients and ecosystem might respond to changes in source nutrients for comparison with the model sensitivity experiments carried out in this study (Dugdale *et al.*, 2002). The source $Si(OH)_4$ increased dramatically from a minimum of 6 [mmolSi m^{-3}] in early October to a maximum of 13 [mmolSi m^{-3}] by October 16, 1992, while the source NO_3 concentration varied from a low of 10 [mmolN m^{-3}] to a maximum of 14 [mmolN m^{-3}] (Fig. 11 (c), (d)). Large increases in chlorophyll concentration and net community production, particularly for diatoms, were observed during this event (Fig. 11 (a) and (b); Iriarte and Fryxell, 1995; Barber *et al.*, 1996).

We compared the model results in Experiment 2 with the JGOFS TT012 cruise data during the passage of the TIWs (Fig. 12). Because the source $Si(OH)_4$ concentration was enhanced by the TIWs (Fig. 12 (d)), the x-axes in Fig. 12 clearly correspond to the time series. The profiles of state variables in the surface water vs. source $Si(OH)_4$ concentrations showed that the model results well captured the observed features during the passage of the TIWs, such as a linear surface $Si(OH)_4$ increase with source $Si(OH)_4$ increase (Fig. 12 (b)), and maxima of surface NO_3, TCO_2, and pCO_{2sea} at intermediate source $Si(OH)_4$ concentrations (Fig. 12 (a), (c), (d)). The maxima of surface NO_3, TCO_2, and pCO_{2sea} were regarded as results of increases and decreases in these state variables during and after the passage of the TIWs, respectively.

The model results with each source $Si(OH)_4$ concentration in Experiment 2 were obtained by establishing steady states, running the model for 1000 days. Therefore, the model results in Experiment 2 may not reproduce the observed rapid increases in phytoplankton growth and chlorophyll concentration in response to the TIWs (Fig. 11 (a), (b)). We hypothesize that this is because the dramatic changes in phytoplankton growth and biomass would be caused by non steady-state biological

responses to the passage of the TIWs, which may not be reproduced by Experiment 2.

5. Concluding remarks

To understand factors and mechanisms controlling carbon and silicon cycling in the equatorial Pacific upwelling region, an ecosystem model with coccolithophorids and its calcification processes has been constructed. We examined biogeochemical responses to the tropical instability waves with increases of source (120m depth) $Si(OH)_4$ concentration. The model results revealed the top-down control (grazing by zooplankton) on phytoplankton biomass and bottom-up control (nutrient limitations, especially $Si(OH)_4$ limitation on diatom growth) on phytoplankton growth.

The model sensitivity study to the increase of source (120m depth) $Si(OH)_4$ concentration showed linear increase in surface diatoms and biogenic silica export, decrease in surface picoplankton, and a maximum surface coccolithophorids at intermediate source $Si(OH)_4$ concentrations. Surface total alkalinity and total CO_2 had the minimum and maximum, respectively, at intermediate source $Si(OH)_4$ concentrations, which produced highest CO_2 release to the atmosphere with the source $Si(OH)_4$ concentration of 7.5 [mmolSi m^{-3}]. The export ratio of PIC to particulate organic carbon (rain ratio) at 120m depth had its maximum of 0.16 with the source $Si(OH)_4$ concentration of 7.5 [mmolSi m^{-3}], suggesting a significant PIC sedimentation in the equatorial Pacific upwelling region. Enhanced change in biogenic silica export flux than in surface diatom biomass suggests that sedimented detritus under the region acts as an amplifier of changes in surface properties.

Comparison between calcification and no-calcification model results revealed that the presence of coccolithophorids persistently elevated diatom biomass and export fluxes of detritus while it decreased total alkalinity and enhanced CO_2 release to the atmosphere. Large changes in the carbonate system in responses to source $Si(OH)_4$ concentrations suggest that physical forcing, such as the tropical instability waves, Kelvin waves, and La Niña, significantly affect the carbon and silicon fluxes in the region.

To better understand the carbon and silicon cycling in the equatorial Pacific upwelling region, we need more information on the processes regulating calcifiers and PIC, not only in the surface but also in the subsurface layer where the calcification is considered significant.

Acknowledgements. The authors thank two anonymous reviewers for improving the manuscript, and Drs. Richard Dugdale, Richard Barber, and Tsung-Hung Peng for the discussion on comparison with observations in the equatorial Pacific. Funding for this work was provided to F. Chai by a NSF grant (OCE-0137272) and a NASA grant (NAG5-9348) and to M. Fujii by MEXT through Special Coordination Funds for Promoting Science and Technology.

Appendix

A.1 Governing equations

The model equations describing each compartment all take the form:

$$\frac{\partial C_i}{\partial t}[mmol\ m^{-3}\ day^{-1}] = PHYSICS(C_i) + BIOLOGY(C_i), \quad \text{(A1)}$$

i = 1, …, 13.

The term PHYSICS(C_i) represents the contribution to the concentration change due to physical processes, including vertical advection and eddy diffusion:

$$PHYSICS(C_i)\,[mmol\ m^{-3}\ day^{-1}] = \underbrace{-W\frac{\partial C_i}{\partial z}}_{advection} + \underbrace{\frac{\partial}{\partial z}(A_{Tv}\frac{\partial C_i}{\partial z})}_{eddy\ diffusivity}, \quad \text{(A2)}$$

where W is vertical velocity, and A_{Tv} is vertical coefficient. The term BIOLOGY (Ci) represents biological sources and sinks of that compartment. In the euphotic zone (the upper 120m), the biological terms, BIOLOGY(Ci) are:

$$BIOLOGY(P1)\,[mmolN\ m^{-3}\ day^{-1}] = \underbrace{NP1 + RP1}_{growth} - \underbrace{G_1}_{grazing\ by\ Z1}, \quad \text{(A3)}$$

$$BIOLOGY(P2)\,[mmolN\ m^{-3}\ day^{-1}] = \underbrace{NP2 + RP2}_{Growth} - \underbrace{G_2}_{grazing\ by\ Z2} - \underbrace{\gamma_3 P2}_{mortality} - \underbrace{\frac{\partial}{\partial z}(W_1 P2)}_{\text{sin}\,king}, \quad \text{(A4)}$$

$$BIOLOGY(P3)\,[mmolN\ m^{-3}\ day^{-1}] = \underbrace{NP3 + RP3}_{growth} - \underbrace{G_5}_{grazing\ by\ Z2} - \underbrace{\gamma_6 P3}_{mortality} - \underbrace{\frac{\partial}{\partial z}(W_3 P3)}_{\text{sin}\,king}, \quad \text{(A5)}$$

$$BIOLOGY(Z1)\,[mmolN\ m^{-3}\ day^{-1}] = \underbrace{G_1}_{grazing\ on\ P1} - \underbrace{G_3}_{predation\ by\ Z2} - \underbrace{reg_1 Z1}_{excretion}, \quad \text{(A6)}$$

$$BIOLOGY(Z2)\,[mmolN\,m^{-3}\ day^{-1}] = \underbrace{\gamma_1\,(G_2+G_3+G_4+G_5)}_{fecal\ pullet} - \underbrace{reg_2 Z2}_{excretion} - \underbrace{\gamma_2 Z2^2}_{loss}, \tag{A7}$$

$$BIOLOGY(NO_3)\,[mmolN\,m^{-3}\ day^{-1}] = - \underbrace{NP1}_{uptake\ by\ P1} - \underbrace{NP2}_{uptake\ by\ P2} - \underbrace{NP3}_{uptake\ by\ P3} + \underbrace{\gamma_5 NH_4}_{nitrification}, \tag{A8}$$

$$\begin{aligned} BIOLOGY(NH_4)\,[mmolN\,m^{-3}\ day^{-1}] = &- \underbrace{RP1}_{uptake\ by\ P1} - \underbrace{RP2}_{uptake\ by\ P2} - \underbrace{RP3}_{uptake\ by\ P3} \\ &+ \underbrace{reg_1 Z1 + reg_2 Z2}_{excretion} + \underbrace{\gamma_7 PON}_{PON\ remineralization} - \underbrace{\gamma_5 NH_4}_{nitrification}, \end{aligned} \tag{A9}$$

$$BIOLOGY(Si(OH)_4)\,[mmolSi\,m^{-3}\ day^{-1}] = - \underbrace{R_{SiN}(NP2+RP2)}_{silicification} + \underbrace{\gamma_4 bSiO_2}_{bSiO2\ dissolution}, \tag{A10}$$

$$\begin{aligned} BIOLOGY(PON)\,[mmolN\,m^{-3}\ day^{-1}] = &\underbrace{(1-\gamma_1)\,(G_2+G_3+G_4+G_5)}_{fecal\ pullet} - \underbrace{G_4}_{grazing\ by\ Z2} + \underbrace{\gamma_3 P2}_{P2\ mortality} \\ &+ \underbrace{\gamma_6 P3}_{P3\ mortality} - \underbrace{\gamma_7 PON}_{PON\ remineralization} - \underbrace{\frac{\partial}{\partial z}(W_2 PON)}_{sinking}, \end{aligned} \tag{A11}$$

$$BIOLOGY(bSiO_2)\,[mmolSi\,m^{-3}\ day^{-1}] = \underbrace{R_{SiN}\,G_2}_{fecal\ pullet} - \underbrace{\gamma_4 bSiO_2}_{dissolution} + \underbrace{\gamma_3 R_{SiN} P2}_{P2\ mortality} - \underbrace{\frac{\partial}{\partial z}(W_4 bSiO_2)}_{sinking}, \tag{A12}$$

$$BIOLOGY(PIC)\,[mmolC\,m^{-3}\ day^{-1}] = \underbrace{R_{CN}\varepsilon G_5}_{fecal\ pullet} - \underbrace{\gamma_8 PIC}_{dissolution} + \underbrace{\gamma_6 R_{CN}\varepsilon P3}_{P3\ mortality} - \underbrace{\frac{\partial}{\partial z}(W_5 PIC)}_{sinking}. \tag{A13}$$

Each biological process is described in next subsection. See Table 1 for abbreviations.

PIC production reduces TAlk, and PIC dissolution increases TAlk (*e.g.* Broecker and Peng, 1982). Brewer and Goldman (1976) demonstrated that the phytoplankton growth could affect TAlk through nutrient uptake of nutrients as well. Uptake of NO_3 caused an increase in TAlk, whereas uptake of NH_4 produced a decrease. This is because one mole of NO_3 assimilation by phytoplankton generates one equivalent of strong base (OH^-), and for NH_4, one equivalent of strong acid (H^+). Therefore, the biological term for TAlk is written as follows:

$$BIOLOGY(TAlk)\,[mmol\,m^{-3}\ day^{-1}] = 2.0 \times \left\{ \underbrace{\gamma_8 PIC}_{PIC\ dissolution} - \underbrace{R_{CN}\varepsilon(NP3 + RP3)}_{calcification} \right\} - BIOLOGY(NO_3) + BIOLOGY(NH_4). \quad \text{(A14)}$$

The photosynthesis and calcification are associated with a decrease in TCO_2. The distribution of TCO_2 in the water column can be given as

$$\frac{\partial(TCO_2)}{\partial t}\,[mmolC\ m^{-3}\ day^{-1}] = PHYSICS(TCO_2) + BIOLOGY(TCO_2) + EVASION(TCO_2), \quad \text{(A15)}$$

$$BIOLOGY(TCO_2)\,[mmolC\,m^{-3}\ day^{-1}] = \underbrace{\gamma_8 PIC}_{PIC\ dissolution} - \underbrace{R_{CN}\varepsilon(NP3 + RP3)}_{calcification} + R_{CN}BIOLOGY(NO_3) + R_{CN}BIOLOGY(NH_4), \quad \text{(A16)}$$

$$EVASION(TCO_2)\,[mmolC\,m^{-3}\ day^{-1}] = E\Delta pCO_2, \quad \text{(A17)}$$

where E is the mean CO_2 exchange coefficient of 0.0391 [mmolC m^{-3} day^{-1} ppm^{-1}] at partial pressure of CO_2 (pCO_2) of 280ppm, and ΔpCO_2 is the difference in pCO_2 between surface water and atmosphere. The atmospheric pCO_2 is assumed to be constant at 357ppm (Chai *et al.*, 2002). The EVASION (TCO_2) term is only applied to the surface level, and is equal to zero in the water column below surface level.

A.2 Formulation of biological processes

(Irradiance)

$$I\,[\mathrm{W\ m^{-2}}] = I_0\ \exp\left\{-k_1 z - k_2 \int_{-z}^{0} (P1 + P2 + P3)dz\right\}, \tag{A18}$$

$$I_0\,[\mathrm{W\ m^{-2}}] = \begin{cases} I_0^{Noon} \sin\left(\frac{t-6}{12}\pi\right) & \text{(from 6 am to 6 pm),} \\ 0 & \text{(from 6 pm to 6am),} \end{cases} \tag{A19}$$

where I_o^{Noon} is the averaged surface noontime irradiance (410 [W m^{-2}]; Chai *et al.*, 2002).

(NO_3 uptake by picoplankton)

$$NP1\,[\mathrm{mmolN\ m^{-3}\ day^{-1}}] = \mu 1_{max} \underbrace{\frac{NO_3}{K_{NO_3} + NO_3}}_{NO_3\ \text{regulation}} \underbrace{e^{-\Psi NH_4}}_{NH_4\ \text{inhibition}} \underbrace{(1 - e^{-\frac{\alpha}{\mu 1_{max}} I})}_{\text{light regulation}} P1. \tag{A20}$$

(NH_4 uptake by picoplankton)

$$RP1\,[\mathrm{mmolN\ m^{-3}\ day^{-1}}] = \mu 1_{max} \underbrace{\frac{NH_4}{K_{NH_4} + NH_4}}_{NH_4\ \text{regulation}} \underbrace{(1 - e^{-\frac{\alpha}{\mu 1_{max}} I})}_{\text{light regulation}} P1. \tag{A21}$$

(NO_3 and NH_4 uptake by diatoms)

$$\text{If } \frac{1}{R_{SiN}} \frac{Si(OH)_4}{K_{Si(OH)_4} + Si(OH)_4} > \frac{NH_4}{K_{P2\_NH_4} + NH_4},$$

$$NP2\,[mmolN\ m^{-3}\ day^{-1}] = \mu 2_{\max} \left\{ \underbrace{\frac{1}{R_{SiN}} \frac{Si(OH)_4}{K_{Si(OH)_4} + Si(OH)_4}}_{Si(OH)_4\ regulation} - \underbrace{\frac{NH_4}{K_{P2\_NH_4} + NH_4}}_{NH_4\ regulation} \right\} \times \underbrace{(1 - e^{-\frac{\alpha}{\mu 2_{\max}} I})}_{light\ regulation} P2, \quad \text{(A22)}$$

$$\mathrm{RP2\,[mmolN\ m^{-3}\ day^{-1}] = \mu 2_{max}} \underbrace{\frac{\mathrm{NH_4}}{\mathrm{K_{P2\_NH_4} + NH_4}}}_{\mathrm{NH_4\ regulation}} \underbrace{(1 - \mathrm{e}^{-\frac{\alpha}{\mu 2_{\max}} \mathrm{I}})}_{\text{light regulation}} \mathrm{P2}. \quad \text{(A23)}$$

If $\frac{1}{R_{SiN}} \frac{Si(OH)_4}{K_{Si(OH)_4} + Si(OH)_4} \le \frac{NH_4}{K_{P2\_NH_4} + NH_4}$,

$$\mathrm{NP2} = 0, \quad \text{(A24)}$$

$$RP2 = \mu 2_{\max} \frac{1}{R_{SiN}} \frac{Si(OH)_4}{K_{Si(OH)_4} + Si(OH)_4} \underbrace{(1 - e^{-\frac{\alpha}{\mu 2_{\max}} I})}_{light\ regulation} P2. \quad \text{(A25)}$$

(NO_3 uptake by coccolithophorids)

$$\mathrm{NP3\,[mmolN\ m^{-3}\ day^{-1}] = \mu 3_{max}} \underbrace{\frac{\mathrm{NO_3}}{\mathrm{K_{P3\_NO_3} + NO_3}}}_{\mathrm{NO_3\ regulation}} \underbrace{\mathrm{e}^{-\Psi \mathrm{NH_4}}}_{\mathrm{NH_4\ inhibition}} \underbrace{(1 - \mathrm{e}^{-\frac{\alpha}{\mu 3_{\max}} \mathrm{I}})}_{\text{light regulation}} \mathrm{P3}. \quad \text{(A26)}$$

(NH_4 uptake by coccolithophorids)

$$\mathrm{RP3\,[mmolN\ m^{-3}\ day^{-1}] = \mu 3_{max}} \underbrace{\frac{\mathrm{NH_4}}{\mathrm{K_{P3\_NH_4} + NH_4}}}_{\mathrm{NH_4\ regulation}} \underbrace{(1 - \mathrm{e}^{-\frac{\alpha}{\mu 3_{\max}} \mathrm{I}})}_{\text{light regulation}} \mathrm{P3}. \quad \text{(A27)}$$

(Grazing on picoplankton by microzooplankton)

$$G_1\ [\mathrm{mmolN\ m^{-3}\ day^{-1}}] = G1_{max}\ \underbrace{\frac{P1}{K1_{gr} + P1}}_{\text{food limitation}}\ \underbrace{\frac{P1}{P1_{ave}}}_{\text{depth modification}}\ Z1, \tag{A28}$$

$$P1_{ave}\ [\mathrm{mmolN\ m^{-3}\ day^{-1}}] = \frac{1}{Z'}\int_{-Z'}^{0} P1 dz, \tag{A29}$$

where Z' is the depth of the euphotic zone (120m).

(Grazing or predation on diatoms, coccolithophorids, microzooplankton, and PON by mesozooplankton)

$$G_2\ [\mathrm{mmolN\ m^{-3}\ day^{-1}}] = G2_{max}\ \frac{\zeta_1 P2}{K2_{gr} + \zeta_1 P2 + \zeta_2 Z1 + \zeta_3 PON + \zeta_4 P3} Z2, \tag{A30}$$

$$G_3\ [\mathrm{mmolN\ m^{-3}\ day^{-1}}] = G2_{max}\ \frac{\zeta_2 Z1}{K2_{gr} + \zeta_1 P2 + \zeta_2 Z1 + \zeta_3 PON + \zeta_4 P3} Z2, \tag{A31}$$

$$G_4\ [\mathrm{mmolN\ m^{-3}\ day^{-1}}] = G2_{max}\ \frac{\zeta_3 PON}{K2_{gr} + \zeta_1 P2 + \zeta_2 Z1 + \zeta_3 PON + \zeta_4 P3} Z2, \tag{A32}$$

$$G_5\ [\mathrm{mmolN\ m^{-3}\ day^{-1}}] = G2_{max}\ \frac{\zeta_4 P3}{K2_{gr} + \zeta_1 P2 + \zeta_2 Z1 + \zeta_3 PON + \zeta_4 P3} Z2, \tag{A33}$$

where

$$\zeta_1 = \frac{\rho_1 P2}{\rho_1 P2 + \rho_2 Z1 + \rho_3 PON + \rho_4 P3}, \tag{A34}$$

$$\zeta_2 = \frac{\rho_2 Z1}{\rho_1 P2 + \rho_2 Z1 + \rho_3 PON + \rho_4 P3}, \tag{A35}$$

$$\zeta_3 = \frac{\rho_3 PON}{\rho_1 P2 + \rho_2 Z1 + \rho_3 PON + \rho_4 P3}, \tag{A36}$$

$$\zeta_4 = \frac{\rho_4 P3}{\rho_1 P2 + \rho_2 Z1 + \rho_3 PON + \rho_4 P3}. \quad \text{(A37)}$$

References

Archer, D., *et al.*, 1997. A meeting place of great ocean currents: shipboard observations of a convergent front at 2°N in the Pacific. Deep-Sea Res. Part II 44(9-10), 1827-1849.

Armstrong, R. A., Lee, C., Hedges, J. I., Honjo, S., Wakeham, S. G., 2002. A new, mechanistic model for organic carbon fluxes in the ocean based on the quantitative association of POC withballast models. Deep-Sea Res. Part II 49, 219-236.

Bacon, M. P., Cochran, J. K., Hirschberg, D., Hammer, T. R., Fleer, A. P., 1996. Export flux of carbon at the equator during the EqPac time-series cruises estimated from ^{234}Th measurements. Deep-Sea Res. Part II 43(4-6), 1133-1153.

Balch, W. M., Kilpatrick, K., 1996. Calcification rates in the equatorial Pacific along 140ºW. Deep-Sea Res. Part II 43 (4-6), 971-993.

Barber, R. T., Sanderson, M. P., Lindley, S. T., Chai, F., Newton, J., Trees, C. C., Foley, D. G., Chavez, F. P., 1996. Primary productivity and its regulation in the equatorial Pacific during and following the 1991-1992 El Niño. Deep-Sea Res. Part II 43 (4-6), 933-969.

Bates, T. S., Cline, J. D., Gammon, R. H., Kelly-Hansen, S., 1987. Regional and seasonal variations in the flux of ocenic dimethylsulfide to the atmosphere. J. Geophys. Res. 92, 2930-2938.

Beucher, C., Tréguer, P., Hapette, A., Corvaisier, R., Metzl, N., Pochon, J., 2004. Intense summer Si-recyling in the surface Southern Ocean. Geophys. Res. Lett. 31, L09305, doi:10.1029/2003GL018998.

Bidigare, R. R., Ondrusek, M. E., 1996. Spatial and temporal variability of phytoplankton pigment distributions in the central equatorial Pacific Ocean. Deep-Sea Res. Part II 43, 809-833.

Bidle, K. D., Azam, F, 1999. Accelerated dissolution of diatom silica by natural marine bacterial assemblages. Nature 397, 508-512.

Bidle, K. D., Manganelli, M., Azam, F., 2002. Regulation of silicon and carbon preservation by temperature control on bacteria, Science 298, 1980-1984.

Bidle, K. D., Brzezinski, M. A., Long, R. A., Jones, J. L., Azam, F., 2003. Diminished efficiency in the silica pump caused by bacteria-mediated silica dissolution. Limnol. Oceanogr. 48, 1855-1868.

Brewer, P. G., Goldman, J. C., 1976. Alkalinity changes generated by phytoplankton growth. Limnol. Oceanogr. 21, 108-117.

Broecker, W. S., Peng, T.-H., 1982. Tracers in the Sea. Lamont-Doherty Geol. Obs., Palisades, New York, 690pp.

Brown, C. W., 1999. Spatial and temporal variability of *Emiliania huxleyi* blooms in SeaWiFS imagery, Eos Trans. AGU, 80(49) Suppl., 153.

Brown, C. W. Yoder, J. A., 1994. Coccolithophorid blooms in the global ocean. J. Geophys. Res. 99, 7467-7482.

Buesseler, K. O., Andrews, J. A., Hartman, M. C., Belastock, R., Chai, F., 1995. Regional estimates of the export flux of particulate organic carbon derived from thorium-234 during the JGOFS EqPac program. Deep-Sea Res. Part II 42(2-3), 777-804.

Buitenhuis, E., Le Quéré, C., Aumont, O., Beaugrand, G., Bunker, A., Hirst, A., Ikeda, T., O'Brien, T., Piontkovski, S., Straile, D., 2006. Biogeochemical fluxes through mesozooplankton. Glob. Biogeochem. Cycles 20, GB2003, doi:10.1029/2005GB002511.

Chai, F., Dugdale, R. C., Peng, T.-H., Wilkerson, F. P., Barber, R. T., 2002. One-dimensional ecosystem model of the equatorial Pacific upwelling system. Part I: model development and silicon and nitrogen cycle. Deep-Sea Res. Part II 49, 2713-2745.

Chai, F., Lindley, S. T., Barber, R. T., 1996. Origin and maintenance of a high nitrate condition in the equatorial Pacific. Deep-Sea Res. Part II, 43(4-6), 1031-1064.

Charlson, R. J., Lovelock, J. E., Andreae, M. O., Warren, S. G., 1987. Oceanic phytoplankton, atmospheric sulphur, cloud albed and climate. Nature 326, 655-661.

Chavez, F. R., Barber, R.T., 1987. An estimate of new production in the equatorial Pacific. Deep-Sea Res. 34, 1229-1243.

Chavez, F. P., Buck, K. R., Coale, K. H., Martin, J. H., DiTullio, G. R., Welshmeyer, N. A., Jacobson, A. C., Barber, R. T., 1991. Growth rates, grazing, sinking and iron limitation of equatorial Pacific phytoplankton. Limnol. Oceanogr. 36, 1816-1833.

Chavez, F.P., Buck, K.R., Service, S.K., Newton, J., Barber, R.T., 1996. Phytoplankton variability in the central and eastern tropical Pacific. Deep-Sea Res. Part II 43, 835-870.

Coale, K. H., Johnson, K. S., Fitzwater, S. E., Gordon, R. M., Tanner, S., Chavez, F. P., Ferioli, L., Sakamoto, C., Rogers, P., Millero, F., Steinberg, P., Nightingale, P., Cooper, D., Cochlan, W. P., Landry, M. R., Constantinou, J., Rollwagen, G., Trasvina, A., Kudela, R., 1996. A massive phytoplankton bloom induced by an ecosystem-scale iron fertilization experiment in the equatorial Pacific Ocean. Nature, 383, 495-501.

Conkright, M. E., Antonov, J. I., Baranova, O., Boyer, T. P., Garcia, H. E., Gelfeld, R., Johnson, D. D., Locarnini, R. A., Murphy, P. P., O'Brien, T. D., Smolyar, I., Stephens, C., 2002. World Ocean Database 2001, Volume 1: Introduction. Ed: S. Levitus, NOAA Atlas, NESDIS 42, U.S. Government Printing Office, Washington, D.C., 167pp.

Deuser, W. G., Ross, E. H., 1989. Seasonally abundant planktonic-foraminifera of the Sargasso Sea : Succession, deep-water fluxes, isotopic compositions, and paleoceanographic implications. J. Foraminiferal Res. 19, 268-293.

Dugdale, R.C., Barber, R. T., Chai, F., Peng, T.-H., Wilkerson, F.P., 2002. One-dimensional ecosystem model of the equatorial Pacific upwelling system. Part II: sensitivity analysis and comparison with JGOFS EqPac data. Deep-Sea Res. Part II 49, 2747-2768.

Dugdale, R.C., Wilkerson, F.P., 1998. Silicate regulation of new production in the equatorial Pacific upwelling. Nature 391, 270-273.

Dugdale, R.C., Wilkerson, F.P., Minas, H. J., 1995. The role of a silicate pump in driving new production. Deep-Sea Res. 42, 697-719.

Dunne, J.P., Murray, J.W., Aufdenkampe, A.K., Blain, S., Rodier, M., 1999. Silicon-nitrogen coupling in the equatorial Pacific upwelling zone, Global Biogeochem. Cycles 13 (3), 715-726.

Fabry, V. J., 1989. Argonite production by pteropod mollusks in the subantarctic Pacific. Deep-Sea Res. 36, 1735-1751.

Feely, R. A., Wanninkhof, R., Goyat, C., Archer, D. E., Takahashi, T., 1997. Variability of CO_2 distributions and sea-air fluxes in the central and eastern equatorial Pacific during the 1991-1994 El Niño. Deep-Sea Res. Part II 44(9-10), 1851-1867.

Flament, P. J., Kennan, S. C., Knox, R. A., Niiler, P. P., Bernstein, R. L., 1996. The three-dimensional structure of an upper ocean vortex in the tropical Pacific ocean, Nature 383, 610-613.

Foley, D. G., Dickey, T. D., McPhaden, M. J., Bidigare, R. R., Lewis, M. R., Barber, R. T., Lindley, S. T., Garside, C., Monov, D. V., McNeil, J. D., 1996. Longwaves and primary productivity variations in the equatorial Pacific at 0ºN, 140ºW. Deep-Sea Res. Part II 44(9-10), 1801-1826.

Francois, R., Honjo, S., Krishfield, R., Manganini, S, 2002. Factors controlling the flux of organic carbon to the bathypelagic zone of the ocean. Global Biogeochem. Cycles 16(4), 1087, doi:10.1029/2001GB011722.

Fujii, M., Chai, F., 2005. Effects of biogenic silica dissolution on silicon cycling and export production. Geophys. Res. Lett. 32, L05617, doi:10.1029/2004GL022054.

Fujii, M., Chai, F., 2007. Influences of initial plankton conditions and mixed layer depth on the outcome of iron-fertilization experiments. submitted to J. Geophys. Res.

Fujii, M., Ikeda, M., Yamanaka, Y., 2005a. Roles of biogeochemical processes in the carbon cycle described with a simple coupled physical-biogeochemical model, J. Oceanogr. 61, 803-815.

Fujii, M., Nojiri, Y., Yamanaka, Y., Kishi, M. J., 2002. A one-dimensional ecosystem model applied to time series station KNOT. Deep-Sea Res. Part II 49, 5441-5461.

Fujii, M., Yamanaka, Y., Nojiri, Y., Kishi, M. J., Chai, F., 2007. Comparison of seasonal characteristics in biogeochemistry among the subarctic North Pacific stations described with a NEMURO-based marine ecosystem model. Ecol. Modell., doi:10.1016/j.ecolmodel.2006.02.046.

Fujii, M., Yoshie, N., Yamanaka, Y., Chai, F., 2005b. Simulated biogeochemical responses to iron enrichments in three high nutrient, low chlorophyll (HNLC) regions, Prog. Oceanogr. 64, 307-324.

Holligan, P. M., Viollier, M., Harbour, D. S., Camus, P., Champagne-Philippe, M., 1983. Satellite and ship studies of coccolithophorid production along a continental shelf edge. Nature 304, 339-342.

Iglesias-Rodríguez, M. D., Brown, C., Doney, S. C., Kleypas, J., Kolber, D., Kolber, Z., Hayes, P. K., Falkowski, P. G., 2002. Representing key phytoplankton functional groups in ocean carbon cycle models: Coccolithophores. Global Biogeochem. Cycles 16, doi:10.1029/001GB001454.

Iriarte, J. L., Fryxell, G. A., 1995. Micro-phytoplankton at the equatorial Pacific (140ºW) during the JGOFS EqPac time series studies: March to April 1992. Deep-Sea Res. Part II 42, 559-584.

Jiang, M.-S., Chai, F., Dugdale, R. C., Wilkerson, F. P., Peng, T.-H., Barber, R. T., 2003. A nitrate and silicate budget in the equatorial Pacific Ocean: a coupled physical-biological model study. Deep-Sea Res. Part II 50, 2971-2996.

Kessler, M. S., McPhaden, M. J., 1995. The 1991-1993 El Niño in the central Pacific. Deep-Sea Res. Part II 42, 295-333.

Ku, T. L., Luo, S., Kusakabe, M., Bishop, J. K. B., 1995. ^{228}Ra-derived nutrient budgets in the upper equatorial Pacific and the role of "new" silicate in limiting productivity, Deep-Sea Res. Part II 42, 479-497.

Landry, M. R., Barber, R. T., Bidigare, R. R., Chai, F., Coale, K. H., Dam, H. G., Lewis, M. R., Lindley, S. T., McCarthy, J. J., Roman, M. R., Stoecker, D. K., Verity, P. G., White, J. R., 1997. Iron and grazing constraints on primary production in the central equatorial Pacific: An EqPac sysnthesis. Limnol. Oceanogr. 42, 405-418.

Landry, M. R., Ondrusek, M. E., Tanner, S. J., Brown, S. L., Constantinou, J., Bidigare, R. R., Coale, K. H., Fitzwater, S., 2000. Biological response to iron fertilization in the eastern equatorial Pacific (IronExII). I. Microplankton community abundances and biomass. Mar. Ecol. Prog. Ser. 201, 27-42.

Le Borgne, R., Bruset, C. Eldin, G., Radenac, M.-H., Rodier, M., 1995. Campagne océanographique FLUPAC à bord du N.O. l'ATALANTE. Du 23 septembre au 29 octobre 1994. Recueil des données, Tome 1. ORSTOM, Nouméa, Archives Sciences de la Mer, Océanographique, No. 1.

Le Borgne, R., Langlade, M. J., Polidori, P., Rodier, M., 1998. Campagne océanographique EBENE à bord du N.O. l'ATALANTE. Du 21 octobre au 20 novembre 1996. Recueil des données, Tome 1. ORSTOM, Nouméa, Archives Sciences de la Mer, Océanographique, No. 3.

Levitus, S., Reid, J. L., Conkright, M. E., Najjar, R., 1993. Distribution of nitrate, phosphate and silicate in the world ocean. Prog. Oceanogr. 31, 245-273.
Leynaert, A., Treguer, P., Lancelot, C., Rodier, M., 2001. Silicon limitation of biogenic silica production in the Equatorial Pacific. Deep-Sea Res. Part I 48, 639-660.
Loukos, H., Frost, B., Harrison, D. E., Murray, J. W., 1997. An ecosystem model with iron limitation of primary production in the equatorial Pacific at 140ºW. Deep-Sea Res. Part II 44(9-10), 2221-2249.
Luo, S., Ku. T.-L., Kusakabe, M., Bishop, J. K. B., Yang, Y.-L., 1995. Tracing particle cycling in the upper ocean with ^{230}Th and ^{228}Th: An investigation in the equatorial Pacific along 140ºW. Deep-Sea Res. Part II 42(2-3), 805-829.
Martin, J. H., et al., 1994. Testing the iron hypothesis in ecosystems of the equatorial Pacific Ocean. Nature 371, 123-129.
McCarthy, J. J., C. Garside, J. L. Nevins, and R. T. Barber (1996), New production along 140W in the equatorial Pacific during and following the 1992 El Niño event, Deep-Sea Res. Part II, 43(4-6), 1065-1093.
Milliman, J. D., Troy, P. J., Balch, W. M., Adams, A. K., Li, Y.-H., MacKenzie, F. T., 1999. Biologically mediated dissolution of calcium carbonate above the chemical lysocline? Deep-Sea Res. Part I 46, 1653-1669.
Moore, J. K., Doney, S. C., Kleypas, J. A., Glover, D. M., Fung, I. Y., 2002. An intermediate complexity marine ecosystem model for the global domain. Deep-Sea Res. Part II 49, 403-462.
Murray, J. W., Johnson, E., Garside, C., 1995. A U.S. JGOFS process study in the equatorial Pacific (EqPac): Introduction. Deep-Sea Res. Part II 42(2-3), 275-293.
Murray, J. W., Leborgne, R., Dandonneau, Y., 1997. JGOFS studies in the equatorial Pacific. Deep-Sea Res. Part II 44(9-10), 1759-1763.
Murray, J.W., Young, J., Newton, J., Dunne, J., Chapin, T., Paul, B., McCarthy, J.J., 1996. Export flux of particulate organic carbon from the central equatorial pacific determined using a combined drifting trap -^{234}Th approach. Deep-Sea Res. Part II 43(4-6), 1095-1133.
Najjar, R. G., Orr, J. C., 1998. Design of OCMIP-2 simulations of chlorofluorocarbons, the solubility pump and common biogeochemistry. 19 pp.
Orr, J., *et al*., 2005. Anthropogenic ocean acidification over the twenty-first century and its impact on calcifying organisms. Nature 437, doi:10.1038/nature04095.
Pasquer, B., Laruelle, G., Becquevort, S., Schoemann, V., Goosse, H., Lancelot, C., 2005. Linking ocean biogeochemical cycles and ecosystem structure and function: results of the complex SWAMCO-4 model. J. Sea Res. 53(1-2), 93-108.
Pätsch, J., Kühn, W., Radach, G., Santana Casiano, J. M., Gonzalez Davila, M., Neuer, S., Freudenthal, T., Llinas, O., 2002. Interannual variability of carbon fluxes at the North Atlantic Station ESTOC. Deep-Sea Res. Part II 49, 253-288.
Price, N. M., Ahner, B. A., Morel, F. M. M., 1994. The equatorial Pacific Ocean: grazer controlled phytoplankton populations in an iron-limited ecosystem. Limnol. Oceanogr. 39, 520-534.
Rainbault, P., Slawyk, G., Boudjellal, B., Coatanoan, C., Conan, P., Coste, B., Garcia, N., Moutin, T., Pujo-Pay, M., 1999. Carbon and nitrogen uptake and export in the equatorial Pacific at 150ºW: evidence of an efficient regenerated production cycle. J. Geophys. Res. 104, 3341-3356.
Riebesell, U., Zondervan, I., Rost, B., Tortell, P. D., Zeebe, R. E., Morel, F. M. M., 2000. Reduced calcification of marine plankton in response to increased atmospheric CO2. Nature 407, 364-367.

Rodier, M., Le Borgne, R., 1997. Export flux of particles at the equator in the western and central Pacific Ocean. Deep-Sea Res. Part II 44, 2085-2113.
Sanderson, M. P., Hunter, C. N., Fitzwater, S. E., Gordon, R. M., Barber, R. T., 1995. Primary productivity and trace metal contamination measurements from a clean rosette system versus ultra-clean Go-Flo bottles. Deep-Sea Res. Part II 42, 431-441.
Sarmiento, J. L., Dunne, J., Gnanadesikan, A., Key, R. M., Matsumoto, K., Slater, R., 2002. A new estimate of the $CaCO_3$ to organic carbon export ratio. Global Biogeochem. Cycles 16, doi:10.1029/2002GB001919.
van Andel, T. H., 1975. Cenozoic history and paleoceanography of the central equatorial Pacific Ocean. Memoirs of the Geological Society of America 143, 1-134.
Walsh, J. J., 1976. Herbivory as a factor in patterns of nutrient utilization in the sea. Limnol. Oceanogr. 21, 1-13.
Westbroek, P., Youn, P. R., Linschooten, K., 1989. Coccolith production (biomineralization) in the marine alga Emiliania huxleyi. J. Protozool. 36, 368-373.
Wyrtki, K., 1981. An estimate of equatorial upwelling in the Pacific. J. Phys. Oceanogr. 11, 1205-1214.
Yamanaka, Y., Tajika, E., 1996. The role of the vertical fluxes of particulate organic matter and calcite in the carbon cycle: Studies using an ocean biogeochemical general circulation model. Global Biogeochem. Cycles 10, 361-382.
Yamanaka, Y., Yoshie, N., Fujii, M., Aita, M. N., Kishi, M. J., 2004. An ecosystem model coupled with nitrogen-silicon-carbon cycles applied to station A7 in the northwestern Pacific. J. Oceanogr. 60, 227-241.
Yoshie, N., Fujii, M., Yamanaka, Y, 2005. Ecosystem changes after the SEEDS iron fertilization in the western North Pacific simulated by a one-dimensional ecosystem model. Prog. Oceanogr. 64, 283-306.

Table 1. The model parameters. Columns (I) and (II) denotes the standard values of parameters in calcification model simulation and no-calcification model simulation, respectively.

Parameters	**Symbol**	**(I)**	**(II)**	**Unit**	**Source**
Light attenuation due to water	k_1	0.046	0.046	m^{-1}	(1)
Light attenuation by phytoplankton	k_2	0.03	0.03	$m^{-1}(mmolNm^{-3})^{-1}$	(1)
Initial slope of the P-I curve	α	0.025	0.025	day^{-1} $(W\ m^{-2})^{-1}$	(1)
Maximum specific growth rate of picoplankton	$\mu 1_{max}$	2.0	2.0	day^{-1}	(1)
NH_4 inhibition parameter	Ψ	5.59	5.59	$(mmolN\ m^{-3})^{-1}$	(1)
Half-saturation for NO_3 uptake by picoplankton	K_{NO3}	1.0	1.0	$mmolN\ m^{-3}$	(1)
Half-saturation for NH_4 uptake by picoplankton	K_{NH4}	0.1	0.1	$mmolN\ m^{-3}$	This study
Maximum specific growth rate of diatoms	$\mu 2_{max}$	3.0	3.0	day^{-1}	(1)
Half-saturation for $Si(OH)_4$ uptake	$K_{Si(OH)4}$	3.0	3.0	$mmolSi\ m^{-3}$	(1)
Half-saturation for NH_4 uptake by diatoms	K_{P2_NH4}	1.0	1.0	$mmolN\ m^{-3}$	(1)
Diatom sinking speed	W_1	1.0	1.0	$m\ day^{-1}$	(1)
Maximum specific growth rate of coccolithophorids	$\mu 3_{max}$	1.0	N/A	day^{-1}	This study
Half-saturation for NO_3 uptake by coccolithophorids	K_{P3_NO3}	1.0	N/A	$mmolN\ m^{-3}$	This study
Half-saturation for NH_4 uptake by coccolithophorids	K_{P3_NH4}	1.0	N/A	$mmolN\ m^{-3}$	This study
Coccolithophorid sinking speed	W_3	1.0	N/A	$m\ day^{-1}$	This study
Microzooplankton maximum specific grazing rate	$G1_{max}$	1.25	1.25	day^{-1}	This study
Half-saturation for microzooplankton ingestion	$K1_{gr}$	0.5	0.5	$mmolN\ m^{-3}$	(1)
Microzooplankton excretion rate to NH_4	reg_1	0.2	0.2	day^{-1}	(1)
Mesozooplankton maximum specific grazing rate	$G2_{max}$	0.48	0.48	day^{-1}	This study
Mesozooplankton assimilation efficiency	γ_1	0.75	0.75		(1)
Half-saturation for mesozooplankton ingestion for diatoms, coccolithophirids, microzooplankton and PON	$K2_{gr}$	0.25	0.25	$mmolN\ m^{-3}$	(1)
Diatom specific mortality rate	γ_3	0.05	0.05	day^{-1}	(1)
Coccolithophorid specific mortality rate	γ_6	0.05	N/A	day^{-1}	This study
Mesozooplankton specific mortality rate	γ_2	0.05	0.05	day^{-1}	(1)
Mesozooplankton excretion rate to NH_4	reg_2	0.1	0.1	day^{-1}	(1)
Grazing preference for diatoms	ρ_1	0.35	0.7	dimensionless	This study
Grazing preference for microzooplankton	ρ_2	0.2	0.2	dimensionless	(1)
Grazing preference for PON	ρ_3	0.1	0.1	dimensionless	(1)
Grazing preference for coccolithophorids	ρ_4	0.35	N/A	dimensionless	This study
PON remineralization rate	γ_7	0.01	0.01	day^{-1}	This study
$bSiO_2$ dissolution rate	γ_4	0.01	0.01	day^{-1}	This study
PIC dissolution rate	γ_8	0.005	N/A	day^{-1}	This study
PON sinking speed	W_2	10.0	10.0	$m\ day^{-1}$	(1)
$bSiO_2$ sinking speed	W_4	20.0	20.0	$m\ day^{-1}$	This study
PIC sinking speed	W_5	20.0	N/A	$m\ day^{-1}$	This study
Diatom Si:N uptake ratio	R_{SiN}	1.5	1.5	$molSi\ (molN)^{-1}$	(2)
Nitrification rate	γ_5	0.025	0.025	day^{-1}	(2)
Ratio of PIC to organic carbon in coccolithophorids	ε	1.0	N/A	$molC\ (olC)^{-1}$	(3)
Ratio of carbon to nitrogen in phytoplankton	R_{CN}	6.625	6.625	$molC\ (molN)^{-1}$	(1)

Sources noted here are: (1) Chai *et al*. (2002); (2) Jiang *et al*. (2003); (3) Fujii *et al*. (2002).

Table 2. Vertically-averaged plankton biomass in the euphotic zone (up to 120m) in (1) calcification model and (2) no-calcification model simulations. Composition ratio of each phytoplankton species to total phytoplankton is shown in percentage term in parentheses.

	Picoplankton (P1) [mmolN m^{-3}]	**Diatoms (P2) [mmolN m^{-3}]**	**Coccolithophorids (P3) [mmolN m^{-3}]**	**Microzooplankton (Z1) [mmolN m^{-3}]**	**Mesozooplankton (Z2) [mmolN m^{-3}]**
(1)	0.15 (63%)	0.06 (24%)	0.03 (13%)	0.13	0.28
(2)	0.17 (77%)	0.05 (23%)	N/A	0.14	0.31

Table 3. Model results in the surface water in (I) calcification model simulation and (II) no-calcification model simulations.

State variable	**(I)**	**(II)**
Picoplankton [mmolN m^{-3}]	0.23	0.36
Diatoms [mmolN m^{-3}]	0.13	0.06
Coccolithophorids [mmolN m^{-3}]	0.06	N/A
Total phytoplankton [mmolN m^{-3}]	0.43	0.42
Microzooplankton [mmolN m^{-3}]	0.35	0.38
Mesozooplankton [mmolN m^{-3}]	0.65	0.89
Total zooplankton [mmolN m^{-3}]	0.99	1.27
NO_3 [mmolN m^{-3}]	6.08	3.56
NH_4 [mmolN m^{-3}]	0.14	0.10
$Si(OH)_4$ [mmolSi m^{-3}]	3.08	5.30
TAlk [mmol m^{-3}]	2360.9	2383.7
TCO_2 [mmolC m^{-3}]	2045.9	2034.5
pCO_{2sea} [µatm]	401.0	353.5
Picoplankton specific growth rate [day^{-1}]	1.01	0.97
Diatom specific growth rate [day^{-1}]	0.45	0.55
Coccolithophorid specific growth rate [day^{-1}]	0.24	N/A
Specific grazing rate on picoplankton by microzooplankton [day^{-1}]	0.95	0.92
Specific grazing rate on diatoms by mesozooplankton [day^{-1}]	0.23	0.30
Specific grazing rate on coccolithophorids by mesozooplankton [day^{-1}]	0.10	N/A
Specific predation rate on microzooplankton by mesozooplankton [day^{-1}]	0.32	0.51
Specific grazing rate on PON by mesozooplankton [day^{-1}]	0.02	0.04

Table 4. Comparison of export fluxes and ratios at the bottom of euphotic zone (120m depth).

Experiment	**PON [mmolN m^{-2} day^{-1}]**	**POC [mmolC m^{-2} day^{-1}]**	**$bSiO_2$ [mmolSi m^{-2} day^{-1}]**	**PIC [mmolC m^{-2} day^{-1}]**	**$bSiO_2$:PON ratio**	**PIC:POC ratio**	**Source**
Survey I (TT007)	0.38-0.95	0.6-6.3	0.05-0.1		0.29-0.34		(1),(2),(3),(4)
Time series I (TT008)		1.9-5					(5),(6)
Survey II (TT011)	0.6-4.65	1.5-19.5	0.4-3.9		0.79-1.25		(1),(2),(3),(4)
Time series II (TT012)		2.4					(6)
FLUPAC	2.90±0.65	17.0±2.5		2.3±0.3	0.10-0.23		(7),(8),(3),(4)
OLIPAC	0.68	7.1					(9),(3),(4)
Zonal Flux					0.14-0.45		(3)
EBENE		9-20	2.6				(10),(11)
Model	1.36-1.39	3.8-5.4					(12),(4)
Model	0.76	5.01	2.36	N/A	3.11	N/A	(13)
Model	0.69-0.98	5.04-7.15	0.35-3.20	N/A	0.36-4.64	N/A	(4)
Model (calcification model simulation)	**0.58**	**3.84**	**1.46**	**0.60**	**2.52**	**0.16**	**This study**
Model (no-calcification model simulation)	**0.51**	**3.38**	**0.74**	**N/A**	**1.45**	**N/A**	**This study**

Sources noted here are: (1) Luo *et al.* (1995) ; (2) Murray *et al.* (1996); (3) Dunne *et al*. (1999); (4) Dugdale *et al*. (2002); (5) Buesseler *et al.* (1995); (6) Bacon *et al.* (1996); (7) Le Borgne *et al*. (1995); (8) Rodier and Le Borgne (1997); (9) Rainbault *et al*. (1999); (10) Le Borgne *et al*. (1998); (11) Leynaert *et al*. (2001); (12) Loukos *et al.* (1997); (13) Dugdale and Wilkerson (1998).

Table 5. Sensitivity of surface phytoplankton (P1, P2 and P3 [mmolN m^{-3}]), zooplankton (Z1 and Z2 [mmolN m^{-3}]), nutrients (NO_3 [mmolN m^{-3}], NH_4 [mmolN m^{-3}] and $Si(OH)_4$ [mmolSi m^{-3}]), TAlk [mmol m^{-3}], TCO_2 [mmolC m^{-3}] and pCO_{2sea} [µatm] and of export PON [mmolN m^{-2} day^{-1}], $bSiO_2$ [mmolSi m^{-2} day^{-1}] and PIC [mmolC m^{-2} day^{-1}] fluxes, to biogeochemical parameters in calcification model. Values in parentheses denote model results in the standard experiment. The other values mean difference by changing each parameter value from 0.5 to 1.5 times the standard parameter value. The values in bold letters are those that exceed 100% of each model compartment concentration (10% of those for Talk, TCO_2, and pCO_{2sea}). The parameters in bold letters strongly affect the model results and are described in Section 4.1.

Parameter	**P1 (0.23)**	**P2 (0.13)**	**P3 (0.06)**	**Z1 (0.35)**	**Z2 (0.65)**	**NO_3 (6.08)**	**NH_4 (0.14)**	**$Si(OH)_4$ (3.08)**	**TAlk (2360.9)**	**TCO_2 (2045.9)**	**pCO_{2sea} (401.02)**	**PON (0.58)**	**$bSiO_2$ (1.36)**	**PIC (0.60)**
α	**0.24**	0.08	**0.08**	0.17	**0.75**	**7.84**	0.08	0.53	21.39	80.91	**183.84**	0.19	0.16	0.46
$\mu 1_{max}$	0.20	0.08	**0.08**	0.21	**0.66**	**6.49**	0.08	1.90	33.12	52.64	**147.05**	0.03	0.59	**0.84**
Ψ	0.10	0.03	0.02	0.10	0.41	4.78	0.03	0.72	9.55	56.89	**86.66**	0.13	0.23	0.41
K_{NO3}	0.03	0.01	0.01	0.02	0.08	0.75	0	0.23	3.83	5.83	16.53	0	0.07	0.1
K_{NH4}	0.17	0.05	0.04	0.10	0.50	5.53	0.10	1.50	18.69	47.19	**108.01**	0.05	0.48	0.42
$\mu 2_{max}$	0.09	0.09	0.02	0.01	0.15	1.31	0.03	**3.22**	6.92	10.22	26.92	0.04	0.97	0.19
$K_{Si(OH)4}$	0.02	0.04	0.00	0.01	0.01	0.32	0.01	2.03	0.84	1.33	3.83	0.05	0.63	0.02
K_{S2_NH4}	0.01	0.01	0.01	0.01	0.02	0.16	0.04	0.38	5.20	1.53	5.00	0.02	0.12	0.16
W_1	0.00	0.02	0.00	0.00	0.01	0.02	0.00	0.15	0.13	0.24	0.65	0.03	0.03	0.01
$\mu 3_{max}$	0.15	0.06	**0.11**	0.02	0.32	3.18	0.04	1.44	46.51	14.33	**67.20**	0.09	0.45	**1.37**
K_{S3_NO3}	0.02	0.00	0.01	0.00	0.03	0.22	0.01	0.15	5.52	0.92	6.62	0.01	0.05	0.16
K_{S3_NH4}	0.06	0.02	**0.07**	0.03	0.11	0.71	0.01	0.57	35.24	15.30	26.28	0.09	0.18	**1.08**
W_3	0.02	0.01	0.02	0.00	0.03	0.29	0.01	0.17	4.55	0.25	7.00	0.01	0.06	0.18
$G1_{max}$	**2.04**	**0.15**	**0.11**	0.16	**0.70**	**8.20**	**0.16**	**3.84**	45.39	55.90	**160.23**	0.34	**1.37**	**1.14**
$K1_{gr}$	**0.43**	0.09	**0.11**	0.22	**0.72**	**7.62**	0.09	2.54	43.93	58.95	**174.41**	0.04	0.81	**1.13**
reg_1	0.21	0.03	0.04	0.08	0.29	2.79	0.01	1.01	17.43	46.01	**112.43**	0.02	0.33	0.46
$G2_{max}$	**1.02**	**0.45**	**1.12**	0.21	**0.71**	**7.23**	**0.15**	**5.95**	237.68	148.84	**137.18**	**1.74**	**1.75**	**7.25**
$K2_{gr}$	**1.19**	**0.23**	**0.22**	0.31	**0.92**	**7.15**	**0.85**	**5.75**	72.74	36.60	**138.33**	**0.76**	**1.82**	**2.04**
γ_3	0.02	0.02	0.00	0.01	0.02	0.19	0.01	0.57	1.21	2.62	6.66	0.03	0.16	0.04
γ_6	0.05	0.02	0.05	0.02	0.12	0.93	0.01	0.53	15.21	2.43	25.48	0.01	0.17	0.42
γ_2	**0.48**	0.12	**0.09**	0.06	**1.01**	**6.13**	0.09	**3.57**	36.12	55.47	**135.07**	0.15	1.10	**0.92**
reg_2	**0.51**	**0.23**	**0.26**	0.18	**0.77**	**7.51**	**0.15**	**5.08**	85.02	33.55	**114.90**	**0.59**	**1.56**	**2.42**
γ_7	0.00	0.00	0.00	0.00	0.00	1.59	0.01	0.06	1.32	0.78	0.58	0.46	0.02	0.01
γ_4	0.01	0.03	0.00	0.00	0.00	0.15	0.01	0.68	0.30	0.57	1.32	0.02	0.18	0.02
γ_8	0.00	0.00	0.00	0.00	0.00	0.00	0.00	0.00	1.00	0.64	0.30	0.00	0.00	0.14
W_2	0.01	0.00	0.00	0.00	0.04	1.39	0.02	0.02	0.72	1.22	3.05	0.19	0.00	0.06
W_4	0.02	0.04	0.00	0.01	0.02	0.38	0.01	1.14	0.94	1.88	4.76	0.03	1.22	0.02
W_5	0.00	0.00	0.00	0.00	0.00	0.00	0.00	0.00	1.28	0.83	0.40	0.00	0.00	0.48
RSiN	0.08	**0.16**	0.01	0.03	0.19	2.70	0.05	2.97	8.60	15.19	38.69	0.17	0.92	0.17
γ_5	0.00	0.00	0.00	0.00	0.00	0.01	0.02	0.02	1.78	1.21	0.53	0.00	0.01	0.05

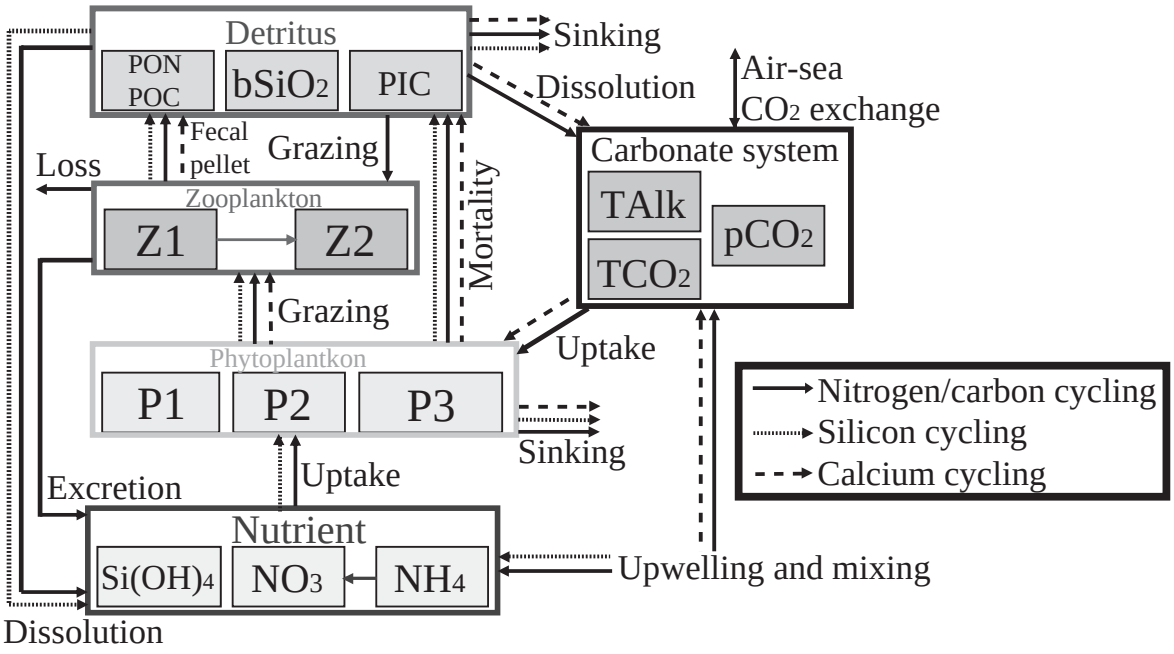

Fig. 1 The inter-compartmental flow chart of the ecosystem and linkage to physical processes. The flows of nitrogen or carbon are indicated by solid lines, the flows of silicon are indicated by dashed lines, and the flows of calcium are indicated by line-dashed lines. P1: picoplankton, P2: diatoms, P3: coccolithophorids, Z1: microzooplankton, and Z2: mesozooplankton.

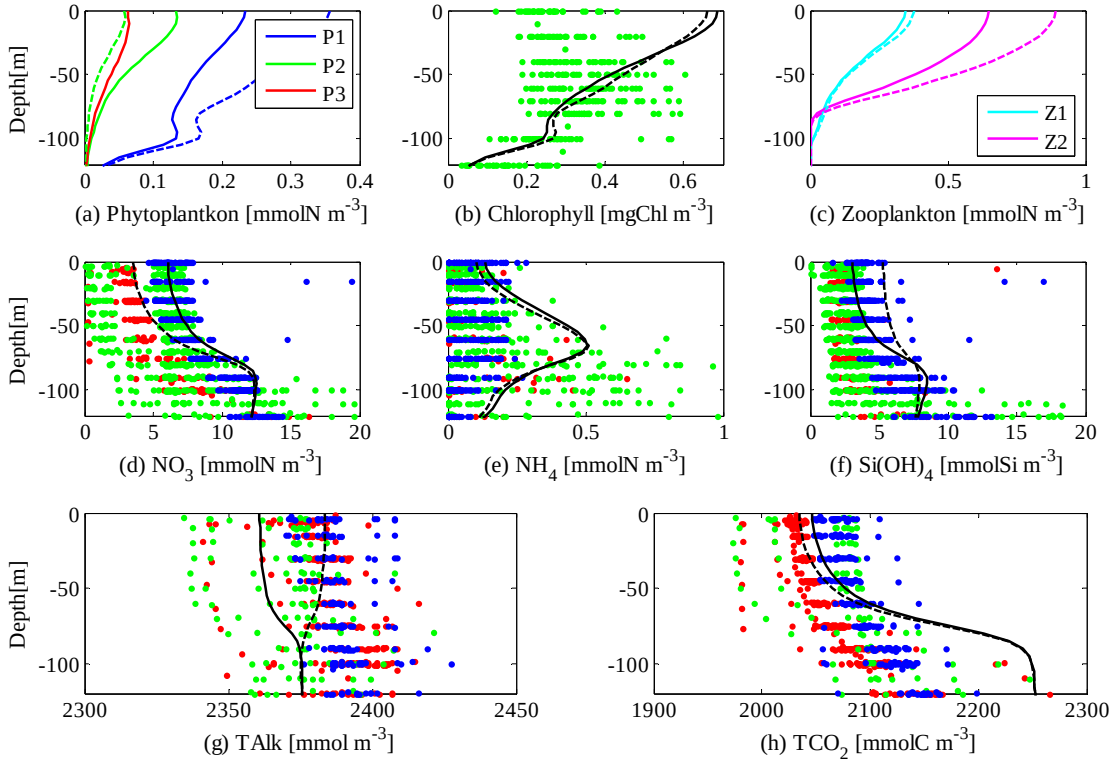

Fig. 2. Modeled vertical profiles of (a) phytoplankton biomass [mmolN m^{-3}], (b) chlorophyll [mgChl m^{-3}], (c) zooplankton biomass [mmolN m^{-3}], (d) NO_3 [mmolN m^{-3}], (e) NH_4 [mmolN m^{-3}], (f) $Si(OH)_4$ [mmolSi m^{-3}], (g) TAlk [mmol m^{-3}], and (h) TCO_2 [mmolC m^{-3}]. Solid lines: calcification model results. Dotted lines: no-calcification model results. Dots denote the JGOFS EqPac data for TT008 (red dots), TT011 (green dots) and TT012 (blue dots).

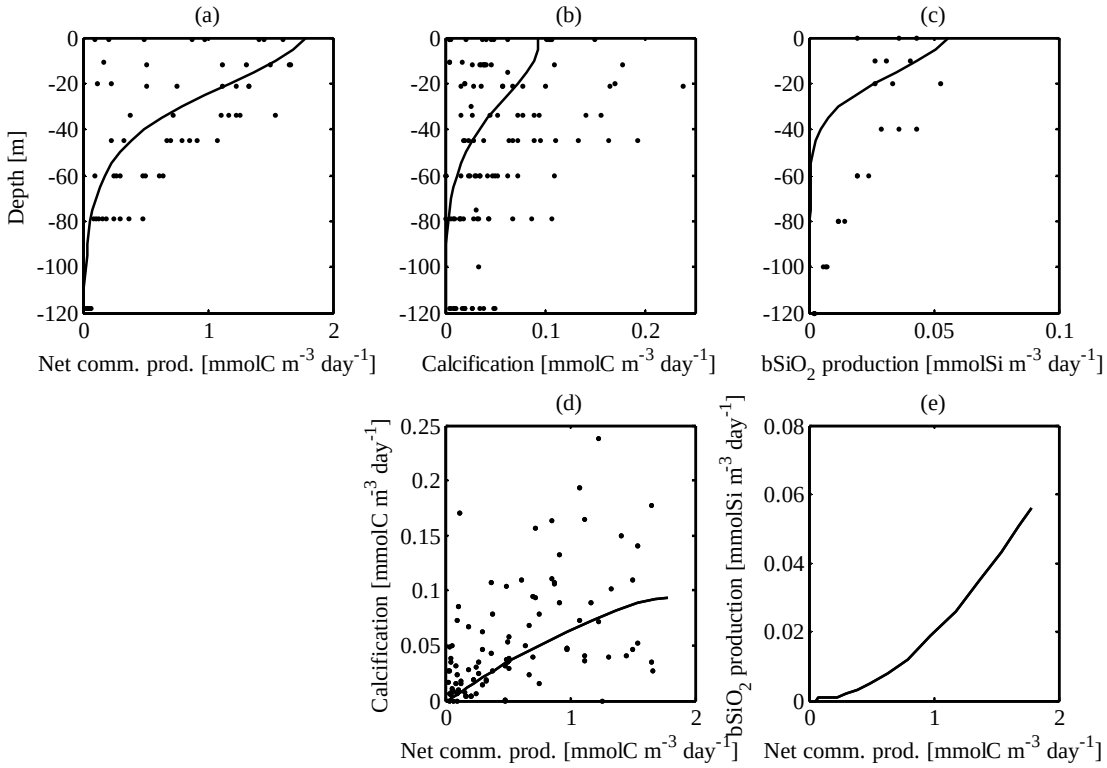

Fig. 3. Modeled (a) vertical profile of net community production [mmolC m^{-3} day^{-1}], (b) vertical profile of calcification [mmolC m^{-3} day^{-1}], (c) vertical profile of $bSiO_2$ production [mmolSi m^{-3} day^{-1}], (d) calcification [mmolC m^{-3} day^{-1}] vs. net community production [mmolC m^{-3} day^{-1}], and (e) $bSiO_2$ production [mmolSi m^{-3} day^{-1}] vs. net community production [mmolC m^{-3} day^{-1}] in the euphotic zone. Dots denote the field observation data from EBENE (Leynaert *et al.*, 2001) for $bSiO_2$ production and EqPac Survey II (TT011) (Balch and Kilpatrick, 1996) for the others.

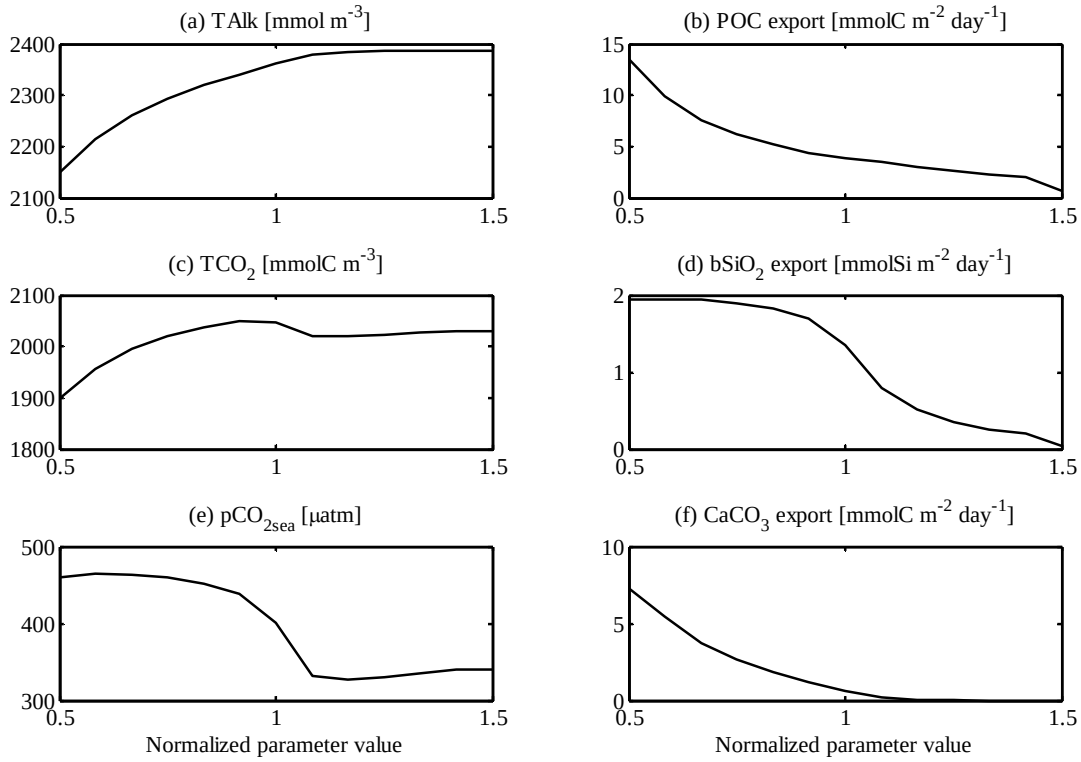

Fig. 4. Modeled (a) surface TAlk [mmol kg^{-3}], (b) export POC flux [mmolC m^{-2} day^{-1}] at 120m depth, (c) surface TCO_2 [mmolC m^{-3}], (d) export $bSiO_2$ flux [mmolSi m^{-2} day^{-1}] at 120m depth, (e) pCO_{2sea} [µatm], and (f) export PIC flux at 120m depth [mmolC m^{-2} day^{-1}], obtained by changing the maximum grazing or predation rate by mesozooplankton ($G2_{max}$) from 0.5 to 1.5 times the standard value.

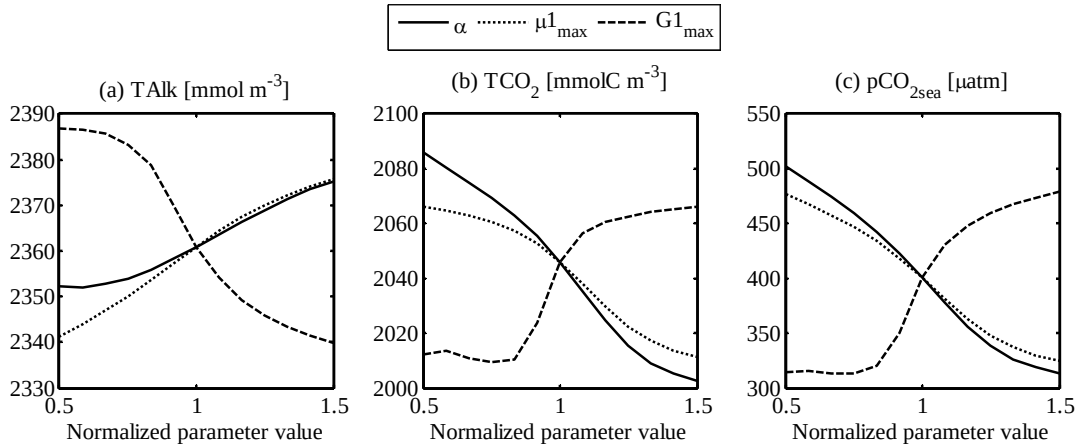

Fig. 5. Modeled (a) surface TAlk [mmol m^{-3}], (b) surface TCO_2 [mmolC m^{-3}], and (c) pCO_{2sea} [μatm], obtained by changing the initial slope of P-I curve (α), the maximum specific growth rates of picoplankton ($\mu 1_{max}$), and the maximum specific grazing rate on picoplankton by mesozooplankton ($G1_{max}$) from 0.5 to 1.5 times the standard value.

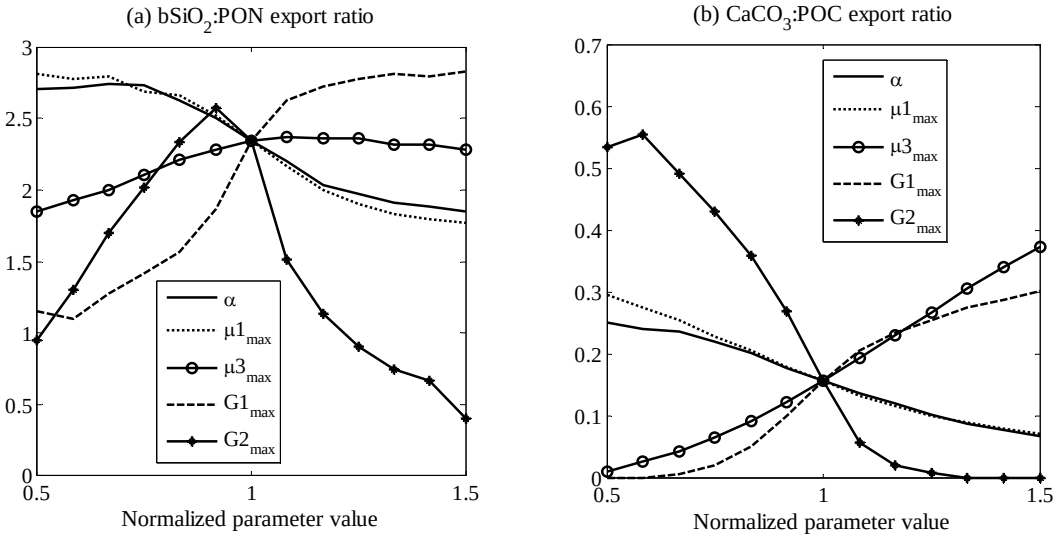

Fig. 6. Modeled (a) $bSiO_2$:PON export ratio and (b) PIC:POC export ratio (rain ratio) at 120m depth, obtained by changing the initial slope of P-I curve (α), the maximum specific growth rates of picoplankton ($\mu 1_{max}$) and coccolithophorids ($\mu 3_{max}$), the maximum specific grazing or predation rates by mesozooplankton ($G1_{max}$) and mesozooplankton ($G2_{max}$) from 0.5 to 1.5 times the standard values.

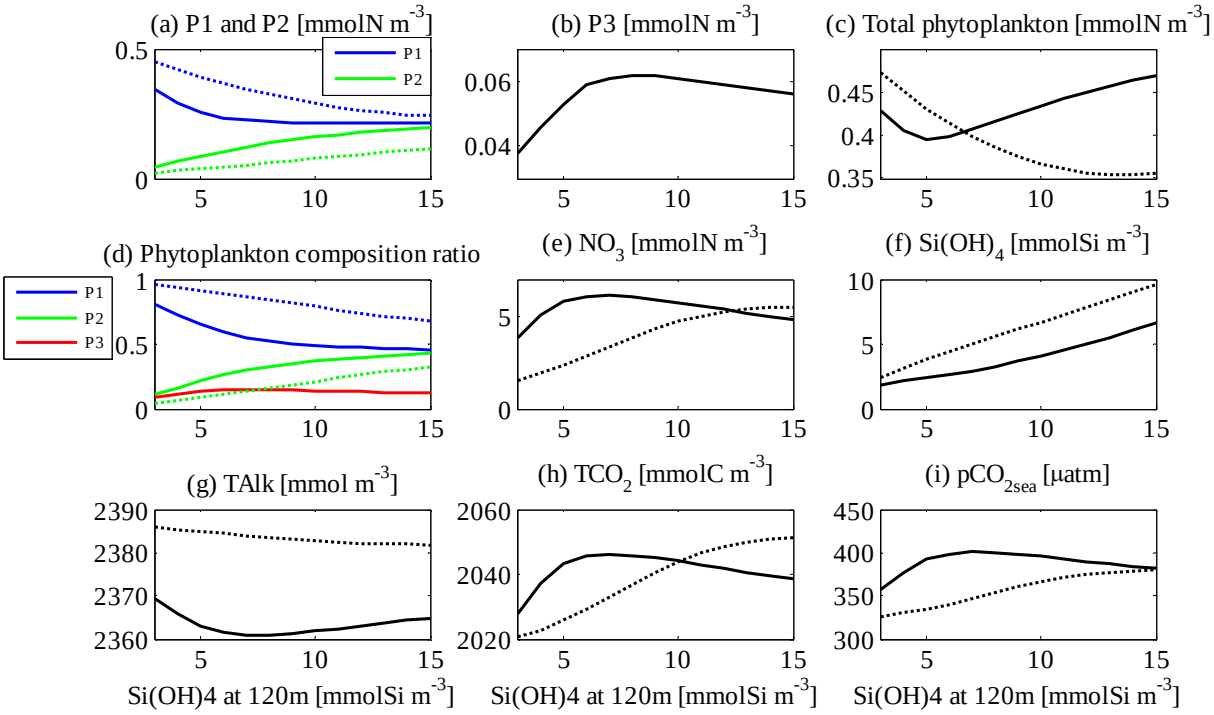

Fig. 7 Modeled surface (a) picoplankton (P1; in blue) and diatom (P2; in green) [mmolN m^{-3}], (b) coccolithophorids (P3) [mmolN m^{-3}], (c) total phytoplankton (P1+P2+P3 for calcification model simulation and P1+P2 for no-calcification model simulation) [mmolN m^{-3}], (d) phytoplankton composition ratio of picoplankton (in blue), diatoms (in green), and coccolithophorids (in red) to total phytoplankton, (e) NO_3 [mmolN m^{-3}], (f) $Si(OH)_4$ [mmolSi m^{-3}], (g) TAlk [mmol m^{-3}], (h) TCO_2 [mmolC m^{-3}], and (i) pCO_{2sea} [µatm], vs. source $Si(OH)_4$ concentration [mmolSi m^{-3}] in Experiment 2. Solid lines: calcification model results. Dotted lines: no-calcification model results.

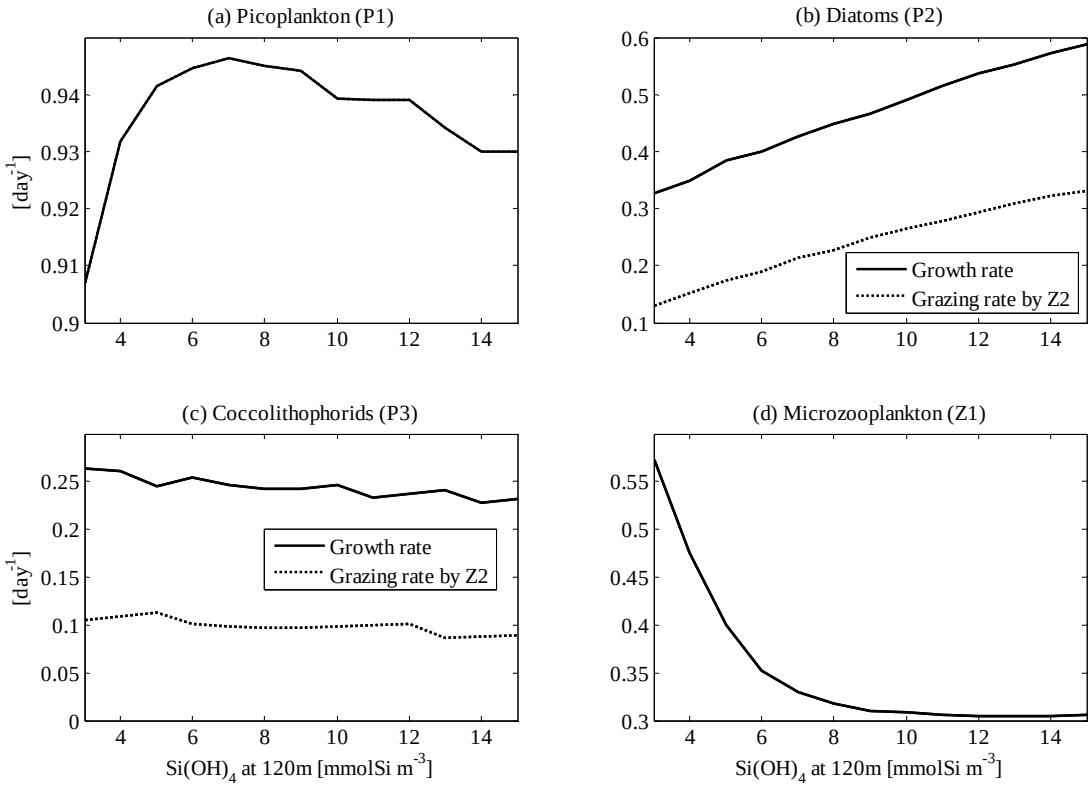

Fig. 8. Modeled specific (divided by each biomass) (a) grazing rate on picoplankton (P1) by microzooplankton (Z1) [day^{-1}], (b) diatom (P2) growth rate and grazing rate by mesozooplankton (Z2) [day^{-1}], (c) coccolithophorid (P3) growth rate and grazing rate by mesozooplankton [day^{-1}], and (d) predation rate on microzooplankton by mesozooplankton [day^{-1}] in the surface water, vs. source $Si(OH)_4$ concentration [mmolSi m^{-3}] in Experiment 2.

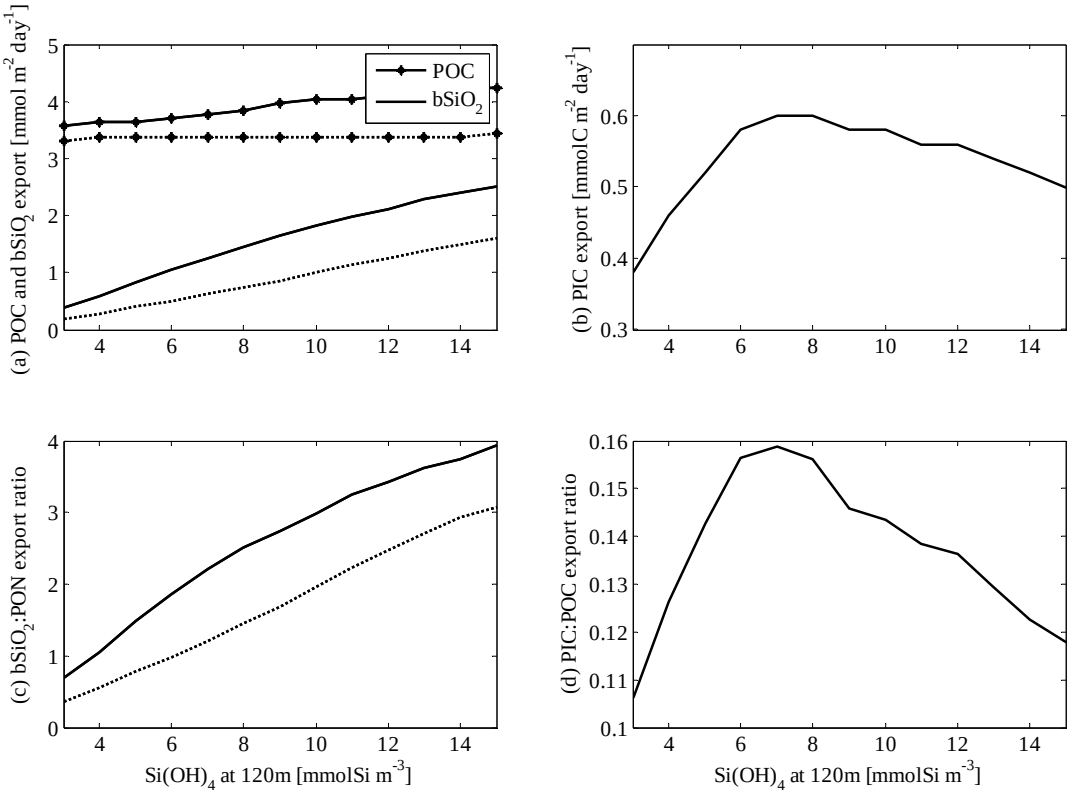

Fig. 9. Modeled (a) export flux of POC [mmolC m^{-2} day^{-1}] and $bSiO_2$ [mmolSi m^{-2} day^{-1}], (b) export PIC flux [mmolC m^{-2} day^{-1}], (c) export $bSiO_2$:PON ratio, and (d) export PIC:POC ratio (rain ratio) at 120m depth vs. source $Si(OH)_4$ concentration [mmolSi m^{-3}] in Experiment 2. Solid lines: calcification model results. Dotted lines: no-calcification model results.

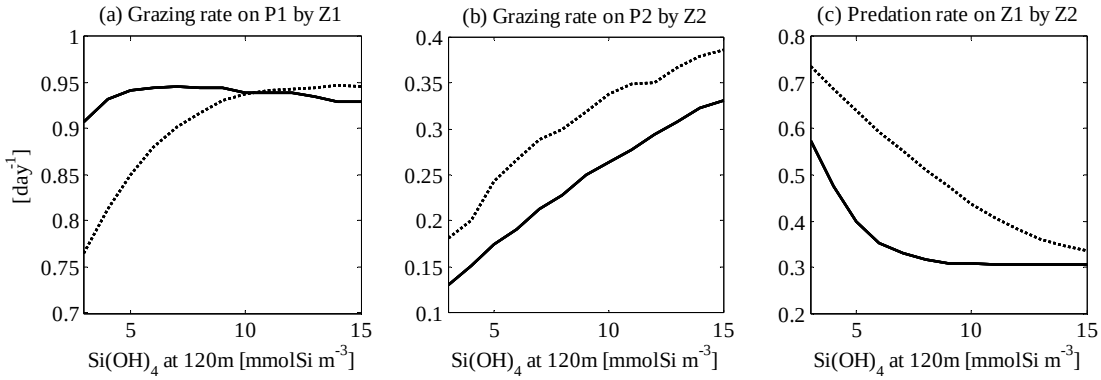

1

2 Fig. 10. Modeled specific (divided by each biomass) (a) grazing rate on picoplankton (P1) by
3 microzooplankton (Z1) [day^{-1}], (b) grazing rate on diatom (P2) by mesozooplankton (Z2) [day^{-1}], and
4 (c) predation rate on microzooplankton (Z1) by mesozooplankton (Z2) [day^{-1}] in the surface water vs.
5 source $Si(OH)_4$ concentration [mmolSi m^{-3}] in Experiment 2. Solid lines: calcification model results.
6 Dotted lines: no-calcification model results.

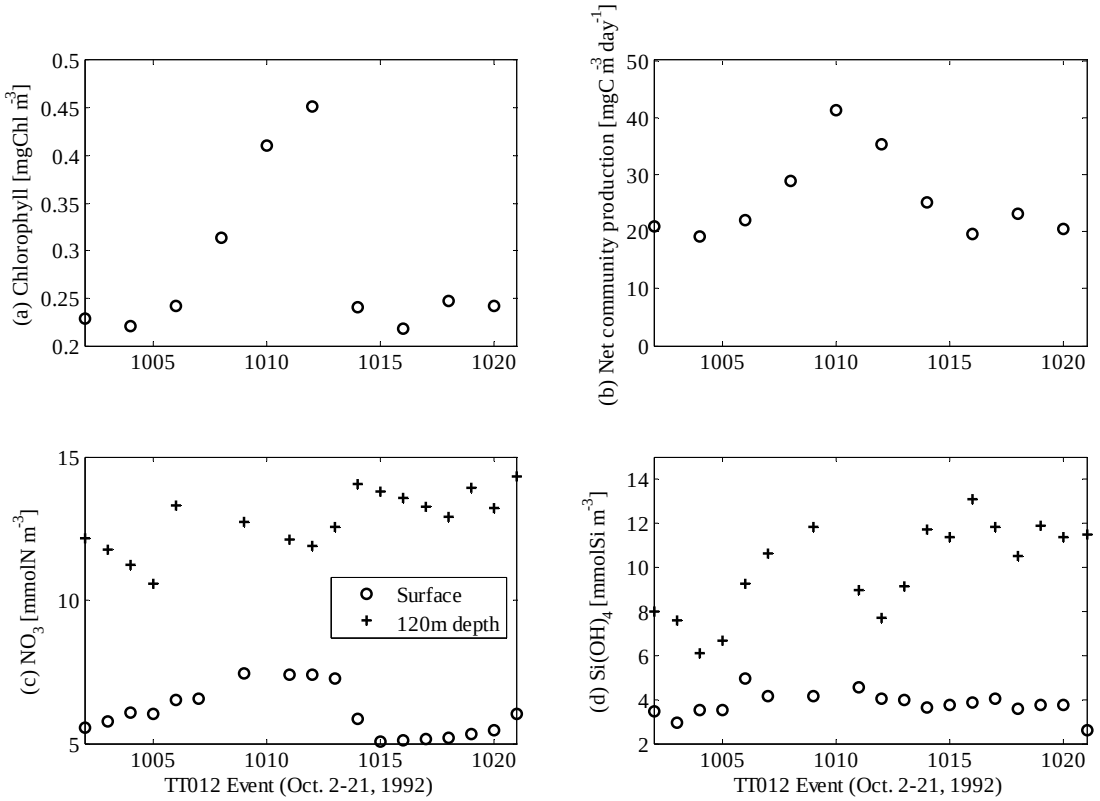

Fig. 11. (a) chlorophyll [mgChl m^{-3}], (b) net community production [mgC m^{-3} day^{-1}], (c) NO_3 [mmolN m^{-3}], and (d) $Si(OH)_4$ [mmolSi m^{-3}] at the surface (open dots) or bottom (crosses) of the euphotic zone (120m depth) during the JGOFS EqPac Time series II (TT012) from Oct. 2 to Oct. 21, 1992.

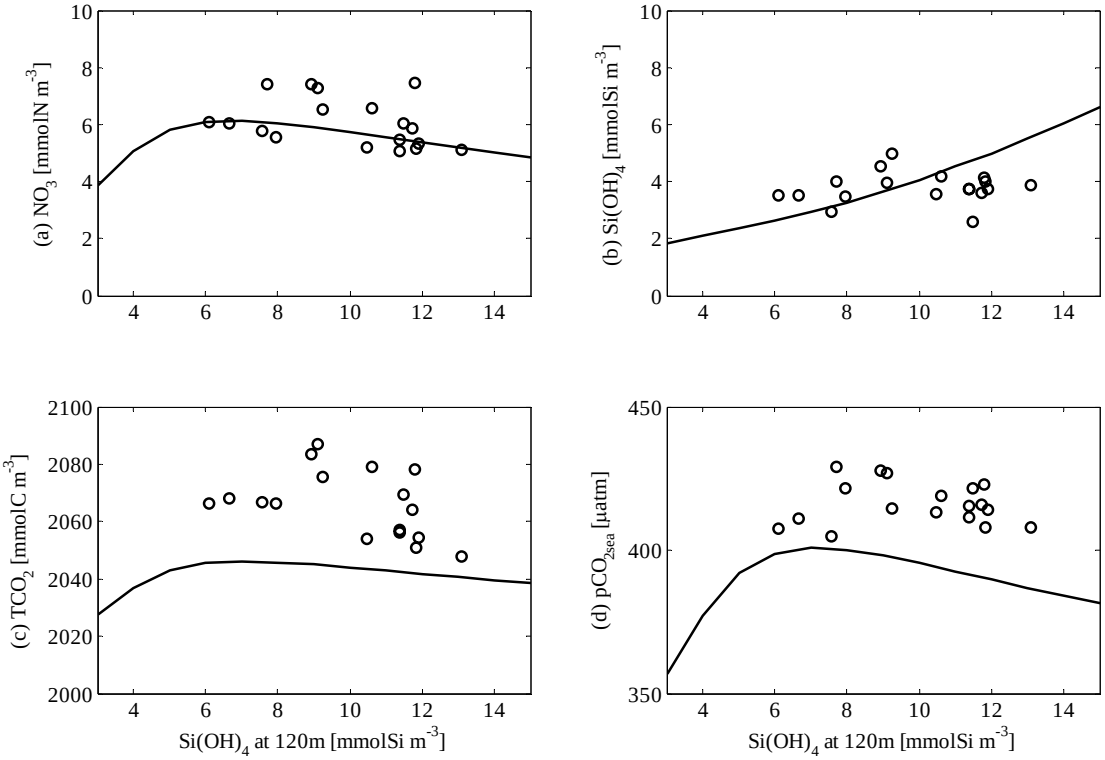

Fig. 12. Surface (a) NO_3 [mmolN m^{-3}], (b) $Si(OH)_4$ [mmolSi m^{-3}], (c) TCO_2 [mmolC m^{-3}] and (d) pCO_{2sea} [µatm] vs. source $Si(OH)_4$ concentration [mmolSi m^{-3}]. Open dots: the JGOFS EqPac Time series II (TT012) data from Oct. 2 to Oct. 21, 1992; Solid lines: calcification model results in Experiment 2.